# NAVAL POSTGRADUATE SCHOOL
## Monterey, California



# THESIS

COMBUSTOR AND NOZZLE EFFECTS
ON PARTICULATE BEHAVIOR
IN SOLID ROCKET MOTORS

by

Bülent Yakin

December, 1993

Thesis Advisor : Professor David W. Netzer

# REPORT DOCUMENTATION PAGE

Form Approved OMB No. 0704-0188



| 1. AGENCY USE ONLY *(Leave blank)* | 2. REPORT DATE | 3. REPORT TYPE AND DATES COVERED |
|---|---|---|
| | December 1993 | Master's Thesis |

**4. TITLE AND SUBTITLE**
Combustor and Nozzle Effects on Particulate Behavior on Solid Rocket Motors.

**5. FUNDING NUMBERS**
F04611-93-X-000505
F04611-93-X-000509

**6. AUTHOR(S)** Bülent YAKIN

**7. PERFORMING ORGANIZATION NAME(S) AND ADDRESS(ES)**
Naval Postgraduate School
Monterey, CA 93943-5000

**8. PERFORMING ORGANIZATION REPORT NUMBER**
-

**9. SPONSORING/MONITORING AGENCY NAME(S) AND ADDRESS(ES)**
Air Force Phillips Laboratory Edwards AFB, CA 93523-5000

**10. SPONSORING/MONITORING AGENCY REPORT NUMBER**
-

**11. SUPPLEMENTARY NOTES**
The views expressed in this thesis are those of the author and do not reflect the official policy or position of the Department of Defense or the U.S. Government.

**12a. DISTRIBUTION/AVAILABILITY STATEMENT**
Approved for public release; distribution is unlimited.

**12b. DISTRIBUTION CODE**
A

**13. ABSTRACT** *(maximum 200 words)*
An investigation was conducted using a subscale solid rocket motor to measure the effect of nozzle residence time on the behavior of $Al_2O_3$ particles to assess the applicability of subscale motor data to full-scale motors and to measure the effects of nozzle entrance particle size distribution on the slag accumulated with submerged nozzles. Although particles as large as 140 μm were present at the nozzle entrance, most of the particulate mass was contained in much smaller particles. This observation is in good agreement with the small mass that accumulated above the submerged nozzle. It was found that both particle breakup and collision coalescence occurred across the exhaust nozzle, with a significant increase in the mass fraction of small (<2 μm) particles. Increasing the nozzle residence time enhanced particle breakup but did not affect the maximum plume particle size. Thus, full-scale motors are expected to have a higher percentage of mass in particles less than 2 μm than subscale motors but with similar diameters of the largest particles.

**14. SUBJECT TERMS**
Particulate, Solid Rockets

**15. NUMBER OF PAGES**
61

**16. PRICE CODE**

| 17. SECURITY CLASSIFICATION OF REPORT | 18. SECURITY CLASSIFICATION OF THIS PAGE | 19. SECURITY CLASSIFICATION OF ABSTRACT | 20. LIMITATION OF ABSTRACT |
|---|---|---|---|
| Unclassified | Unclassified | Unclassified | UL |

NSN 7540-01-280-5500 Standard Form 298 (Rev. 2-89)
Prescribed by ANSI Std. 239-18

Approved for public release; distribution is unlimited.

Combustor and Nozzle Effects on Particulate Behavior
in Solid Rocket Motors

by

Bülent YAKIN
Lieutenant Junior Grade, Turkish Navy
B.S., Turkish Naval Academy, 1986

Submitted in partial fulfillment
of the requirements for the degree of

MASTER OF SCIENCE IN AERONAUTICAL ENGINEERING

from the

NAVAL POSTGRADUATE SCHOOL
December 1993

Author: _____
Bülent YAKIN

Approved by: _____
David W. Netzer, Thesis Advisor

_____
James V. Sanders, Second Reader

_____
Daniel J. Collins, Chairman
Department of Aeronautics and Astronautics

**ABSTRACT**

An investigation was conducted using a subscale solid rocket motor to measure the effect of nozzle residence time on the behavior of $Al_2O_3$ particles to assess the applicability of subscale motor data to full-scale motors and to measure the effects of nozzle entrance particle size distribution on the slag accumulated with submerged nozzles. Although particles as large as 140 μm were present at the nozzle entrance, most of the particulate mass was contained in much smaller particles. This observation is in good agreement with the small mass that accumulated above the submerged nozzle. It was found that both particle breakup and collision coalescence occurred across the exhaust nozzle, with a significant increase in the mass fraction of small (<2 μm) particles. Increasing the nozzle residence time enhanced particle breakup but did not affect the maximum plume particle size. Thus, full-scale motors are expected to have a higher percentage of mass in particles less than 2 μm than subscale motors but with similar diameters of the largest particles.

## TABLE OF CONTENTS

## LIST OF TABLES

## LIST OF FIGURES

# I. INTRODUCTION

Solid propellant rocket motors are relatively simple devices requiring little or no servicing and having no moving parts. This is generally true although in a number of modern systems complicated actuation devices for thrust vector control are included in the basic design.

A rocket motor is a device for converting the thermochemical energy of a propellant into exhaust jet kinetic energy. The propellant for a solid rocket motor is contained and stored directly in the combustion chamber and can remain there for periods of time as long as twenty years in some in-service systems. Figure 1.1 shows a typical solid propellant rocket motor with the various design features indicated [Ref. 1].

Composite solid-propellants typically use aluminum as a fuel and ammonium perchlorate (AP) as the oxidizer. Aluminum is added to increase the delivered specific impulse ($I_{sp}$) and propellant density. The aluminum and AP are mixed together in the form of fine powders in the 10-100 micron size range [Ref. 2]. The size distribution of the powders affects the burn rate, as do burn rate modifiers such as iron oxide and carbon black. During the combustion of aluminized propellants, aluminum oxide particles are formed as one of the major combustion products. Knowledge of the aluminum oxide particle

size distribution and composition is important in order to be able to predict slag formation within the combustion chamber, combustion efficiency, combustion stability, motor performance and insulator erosion" [Ref. 3]. The radiative heating from the flame zone just above the combustion surface of a solid propellant causes the aluminum powder at the propellant surface to melt (933°K) and agglomerate, and the AP/binder to decompose into gaseous products. As the gaseous products leave the surface they carry the agglomerates of molten aluminum/aluminum oxide with them. The aluminum is oxidized on the surface of the agglomerate by $H_2O$, $CO_2$, OH, O, $O_2$ and an oxide $Al_2O_3$ shell or lobe is formed. "Not until the agglomerate reaches the flame zone does the oxide shell compeletly melt (2327°K), whereupon its high surface tension causes it to move to one end of the agglomerate to form a cap" [Ref. 4]. The remainder of the aluminum agglomerate is now free to react with the surrounding gaseous species to form more $Al_2O_3$. This reaction occurs in the vapor phase because the flame temperature (3389°K) exceeds the vaporization temperature (2767°K) of aluminum. The $Al_2O_3$ condenses immediately and either combines with the oxide ca_ or is carried away as small particles/smoke (<2μm) by the gas stream that is rushing past the slow heavy particle. The longer the composite particle experiences this environment, the more Al is oxidized into $Al_2O_3$ cap and smoke. Most motors are long enough and operate at sufficiently high pressure to provide the particles

sufficient residence time in a hot oxidizing environment to allow complete combustion before they reach the aft-end of the chamber. The form/sizes of the final $Al_2O_3$ products depends upon both the time and the local flow environment. Experimental data have indicated that for an average residence time in the combustor ($t_{res}$) less than 10-15 ms, $I_{sp}$ will decrease rapidly due to the incomplete combustion of aluminum [Ref. 5]. For good combustion of aluminum, gas temperatures must also exceed the melting temperature of $Al_2O_3$ (2318°K) and the gas composition must contain enough oxygen-containing species. Thus, high oxidizer levels in propellants are desirable. Some typical data on the effects of $t_{res}$ on $I_{sp}$ efficiency are shown in Figure 1.2 [Ref. 5].

In smaller motors the residence time may be inadequate for complete combustion and unburned aluminum may persist into the nozzle and plume flows. "The observation of green AlO flame bands from small motors, for example, is evidence for incomplete combustion" [Ref. 2]. Since alumina is basically a dielectric material, even small amounts of unburned aluminum may significantly increase the electrical conductivity and the particle emissivity.

The accumulation of alumina slag at the aft-end of large motors which utilize submerged nozzles has been attributed to large (>100μm) particles not being able to track the gas flow into the converging nozzle section [Ref. 4]. However, flow of

surface agglomerates is another possible explanation. In small motors with long residence times aft of the propellant [Ref. 6] large particles (>85 μm) have not been observed at the nozzle entrance. If these measurements are correct and also applicable to large motors, it indicates that alumina particles do not burn entirely in the manner discussed above. Multiple shedding of the $Al_2O_3$ lobe and/or particle-breakup appear to occur even with very low combustor Mach numbers [Ref. 6].

Particle flow in nozzles results in two-phase flow motor performance losses. In addition, the size distribution, temperature and optical properties of the condensed material have a direct effect on the plume signature. Whereas alumina particles in the chamber can exceed 100 microns in diameter, particles collected from plumes are generally micron-sized and seldom larger than about 10-15 microns; because larger particles would not survive the disruptive shear forces in the nozzle throat [Ref. 2]. The acceleration of the gas in the throat is on the order of $10^9$ $cm/s^2$ or equivalently $10^6$ g's. Consequently, in the nozzle throat, aluminum oxide particles much larger than a micron are probably highly irregular and distorted in shape. However, small particles move at higher velocities than do larger particles and this can result in collision coalescence. The latter can increase the particle size through the nozzle. Whether particle-breakup dominates over collisions can also depend upon nozzle residence time. It

takes both the attainment of a critical Weber number and some time period before breakup can occur [Ref. 7]. Large nozzles with the same geometry as small nozzles have much longer particle transit times and, therefore, may produce different plume particle sizes than those from small nozzles. Thus, the length and the shape of the nozzle can also affect the particle size distribution in the plume.

In addition to particle size, one also needs to know exhaust alumina temperatures and phases (i.e., liquid vs. solid). The exhaust alumina temperatures are generally near the melting point. Thus, minor temperature uncertainties which are inconsequential for thrust prediction may have significant consequences for radiation. Alumina temperature and phase will vary with the particle size and position in the plume and they are difficult to predict because the two-phase exhaust is generally not in thermal equilibrium. This typically leads to a several hundred °K thermal lag between the larger droplets and the gas at the nozzle exit plane and, because the flow time scale is shorter in smaller motors, the thermal nonequilibrium is generally more extreme in smaller motors [Ref. 2].

Aluminum in the propellant can also affect the exhaust plume signature by other mechanisms. Particles exhausted by the rocket motor scatter ambient light. This scattering of light forms a visible exhaust called primary smoke. Particles in the exhaust can also scatter light that is radiated from

the combustion chamber. These particles also emit radiation proportional to approximately the fourth power of their surface temperature and proportional to their concentration.

There are several different techniques which have been used to determine the particle size distributions inside the motor chamber or in the plume. The techniques which have been most commonly used are based on electron microscope examination of collected samples. Electron microscope examinations can yield size data as well as particle shape. However, thousands of particles must be measured to obtain an accurate size distribution. In addition, these techniques are intrusive and it is not known how they affect the particle sizes which are measured. To a lesser extent, measurements of the scattering or extinction of light have been used. These techniques are non-intrusive. In one of these techniques, which is currently being used at the Naval Postgraduate School, particle size distributions in the combustor are determined by measuring forward scattered laser light from the ensemble of particles present in a laser beam which is passed through windows on the sides of the combustion chamber. The Malvern 2600 [Ref. 8] is one such device and is based upon Fraunhofer diffraction theory. An interesting approach to the determination of the particle sizes in the combustion chamber has also been discussed by Traineau and associates [Ref. 9]. Traineau injected helium into the combustion chamber to quench aluminum and aluminum oxide particles formed during

combustion. Maintaining the particulate in solid form allowed it to pass through the nozzle and into the exhaust unaltered. Identical tests were then conducted without the helium injection. The particle sizes at the nozzle exit were determined using the measurements of scattered laser light and scanning electron microscope examination of captured particles. Traineau's technique allows the use of exhaust plume diagnostic methods to determine approximately the particle size distribution inside of the combustion chamber, providing that the quench process does not induce particle breakup. Another technique is to use single particle analyzers [Ref. 6]. Recent improvements to the phase-Doppler particle analyzers [Ref.10] may also permit this technique to be successfully used in rocket motors and plumes.

One objective of this investigation was to measure the effect of rocket motor nozzle residence time on the behavior of $Al_2O_3$ particles to assess the applicability of sub-scale motor data to full-scale motors. This was accomplished through the use of nozzles with different converging and diverging half-angles. A second objective was to determine the effects of nozzle entrance particle size distribution on the slag accumulation and nozzle exit particle size distribution of submerged nozzles. A Malvern 2600 HSD particle sizer was used to measure the particle sizes at the nozzle entrance and the nozzle exit. In a related investigation [Ref. 11] a Phase-Doppler Particle Analyzer was used for comparison with the

the Malvern data. The plume thermal image was also recorded for each test to determine if any significant changes in observed particle size distributions would result in significant changes in plume IR signature.

## II. EXPERIMENTAL APPARATUS

### A. BACKGROUND

Two different three dimensional subscale motors, three different types of nozzles (an external nozzle with a 45° converging half-angle and 15° diverging half-angle, a longer external nozzle with converging and diverging half-angles of 20° and 7°, respectively, and a submerged nozzle) and a Malvern 2600 ensemble type particle analyzer were used in this investigation. The plume radiation effects were measured using an AGEMA 870 IR Thermal Imaging Camera [Ref. 12]. Also a software package (LabTech Notebook) was used to control the experiment and measure the pressure-time behavior. Each firing was also recorded by a video camera.

### B. EQUIPMENT

#### 1. Three Dimensional Subscale Motors

Two different solid propellant rocket motors were used to collect data. One of these motors was 2.00 inches in inside diameter, 4.00 inches in outside diameter and 12.25 inches in length. A nitrogen-purged windowed section was attached to the end of this motor to allow measurements with the Malvern 2600 at the nozzle entrance. This windowed section was 2.00 inches in inside diameter and 3.13 inches long. It was utilized with the standard exhaust nozzle (45° converging half-angle and 15°

diverging half-angle). The second motor also had an inside diameter of 2.00 inches but had an outside diameter of 3.27 inches. The combustor length depended upon the nozzle utilized; 10.75 inches with the submerged nozzle and 12.66 inches with the long nozzle. The solid propellant was cut into end-burning cylindrical slabs approximately 2.00 inches in diameter and 1.00 inch thick. All experimental runs, except the initial check-out runs, were conducted using a GAP/AP propellant with 4.7% aluminum (Table I). During the check-out runs a 2% aluminum end-burning grain was used. Nitrogen purge gas was used to keep the fuzed silica windows clean when Malvern 2600 measurements were made at the nozzle entrance. Otherwise, the windows were replaced with stainless steel blanks and the nitrogen purge lines were capped.

Ignition of the propellant was accomplished by using a $BKNO_3$ ignitor which was fired by means of a nichrome filament energized by a 12 volt DC power supply. During the check-out firings a bigger igniter having 0.25 inches inside diameter and 1.00 inches length was used. However it resulted in over-pressurization of the motor and, consequently adequate window purging could not be obtained. Then a standard igniter with 0.195 inches inside diameter and 0.4 inches length was used.

The propellant was bound to the motor casing with a self vulcanizing silicone rubber compound (RTV). This not only

bound the propellant to the casing but also inhibited burning from all surfaces except the exposed end of the grain.

**a. *Subscale Motor with Windows***

The copper exhaust nozzle had a throat diameter of 0.242 inches, a converging half-angle of 45 degrees and a diverging half-angle of 15 degrees (Fig. 2.1). The length of the nozzle was 2.35 inches and the residence time of the particles in the nozzle was calculated to be 0.06 ms. Nitrogen purging was used to keep the windows clean with one 0.035 inch diameter sonic choke and an upstream pressure of 1400 psia. This resulted in a window purge flow rate approximately 9% of the propellant flow rate. The larger nozzle flow rate required a larger throat diameter (0.242") than on non-purged tests in order to obtain the same motor pressure. The igniter port was 2.36 inches from the head-end of the assembled motor and directed at the center of the face of the grain. Figure 2.2 shows the assembled windowed motor used for the experiments.

**b. *Small Subscale Motor***

This motor did not incorporate any windows. Figure 2.3 shows the assembled small subscale motor. Two new nozzles were designed for use with this combustor.

*(1) Long Nozzle.* It was made of copper and was 3.15 inches long with a throat diameter of 0.200 inches. The converging half-angle was reduced to 20 degrees and the diverging half-angle to 7 degrees (Fig 2.4). The residence

diverging half-angle to 7 degrees (Fig 2.4). The residence time of the particles in this nozzle was approximately twice that of the standard nozzle (0.127 msec vs. 0.06 msec). The Space Shuttle booster motor (Fig. 2.5) [Ref. 13] has an approximate nozzle residence time of 3.7 msec.

*(2) Submerged Nozzle.* The Space Shuttle rocket motor exhaust nozzle was also used as the model for the subscale submerged nozzle. It had a total length of 2.130 inches and a throat diameter of 0.200 inches. The converging half-angle was 10 degrees and the diverging half-angle was 15 degrees. The submerged part was rounded off with a radius of 0.120 inches (Fig. 2.6).

**2. Malvern 2600 Particle Sizer**

The Malvern 2600 particle sizer [Ref. 8] uses a 2 mW helium-neon laser operating at $\lambda$=632.8 nm. The laser beam passes from the transmitter with a diameter of 9 mm and is scattered by particles on its way to the receiver. The light scattered by the particles and the unscattered remainder are incident onto a receiver lens, also known as a range lens. This range lens acts as a Fourier transform lens, forming the far field diffraction pattern of the scattered light at its focal plane. The scattered light is then collected over a range of angles by 31 concentric annular photodiode rings. The intensity of light collected by the annular rings is converted into a particle size distribution using Fraunhofer diffraction

theory. The distribution of sizes is for the particles within the volume between the receiver and transmitter. The Malvern 2600 does not depend upon detection of single particles, but rather upon the net scattering of the collection of hundreds to tens of thousands of particles. Thus, the measurements are essentially independent of particle velocity or position. This volumetric sizing technique is often called an ensemble measurement.

For this experiment a 100 mm range lens was used. This lens used forward scattered light with a maximum angle of approximately 9 degrees. This provided a particle size range of 1.9-188 $\mu$m. An estimate of the volume of particles present with diameters between 0.5 and 1.9 $\mu$m is also provided. The vignetting distance associated with this lens is 133 mm.

The accuracy of the Malvern is affected by several conditions. Beam steering from density gradients in the flow causes some difficulties. The correction for beam steering reduces the upper limit of particle size that can be accurately measured. Obscuration also affects the accuracy of the Malvern. Obscurations between 5-50% yield accurate sizes. Obscurations greater than 50% are subject to significant multiple scattering, which causes the Malvern to indicate particle sizes smaller than actually present. Empirical corrections have been developed for high obscuration levels [Ref. 14].

### 3. AGEMA 870 IR Camera

The Agema 870 IR Thermal Imaging Camera was manufactured by AGEMA Infrared Systems [Ref. 12]. It measures in the 3.5-5 microns range. Plume signatures were recorded at an object distance of 1.1 meters. An example of AGEMA data is shown in Figure 2.7.

### 4. Scanning Electron Microscope (SEM)

The basic function of a Scanning Electron Microscope (SEM) is to produce an image of three dimensional appearance derived from the action of an electron beam scanning across the surface of a specimen [Ref. 15]. In this investigation a Stereoscan 200 type SEM was utilized. The resolution under acceptable conditions is greater than 6 nm and the depth of focus is more than 300 times greater than a light microscope. The magnification can be either a few times (10X) or up to several hundred thousand times, limited only by the resolution available. All samples will emit X-rays when struck by the electron beam. These X-rays can be characteristic of the element from which they were emitted. Particles as small as 1 μm can be analyzed.

To examine the slag accumulation around the submerged nozzle the scrapped particles from the vicinity of the submerged nozzle were examined by using the SEM.

## III. EXPERIMENTAL PROCEDURE

### A. PRE-FIRING PREPARATION

Prior to each run the pressure transducer was calibrated by using a dead-weight tester and the LabTech Notebook program.

The end-burning propellant grain was used for all the experiments. The propellant grain was cut from 1" thick slabs to the desired diameter and length. The propellant was then coated with a self-vulcanizing silicone rubber compound (High Temperature RTV) on non-burning surfaces and loaded into the head-end of a clean rocket motor. The motors and their parts needed to be cleaned very carefully after every firing. Otherwise, especially for the windowed motor, it was very hard to keep the windows clean. After at least a 24 hour curing period for the RTV the motor assembly was completed by installing the windowed section, nozzle and burst disk assembly. The motor was then attached to the test stand and the pressure transducer was connected. For the experiments which required motor windows, the windows were not installed until after a nitrogen purge was completed to ensure the nitrogen lines were completely dry. For the experiments that did not require windows, stainless steel slugs were used instead of fused silica windows. The motor was positioned on

the test stand to provide optimum alignment between the motor and the laser for data acquisition. Then nitrogen was set to the desired pressure for window purging. The desired nitrogen gas pressure was taken as at least 2 times that of the chamber pressure. A video camera was used to record all the experiments. The AGEMA 870 IR Camera was also positioned 1.1 meters above the motor to take the IR pictures during the experiments, and the related software package was pre-set. For the Malvern 2600 a background reading was required before the test. The pre-assembled $BKNO_3$ ignitor was then installed and connected to the 12 volt battery power supply. The ignition cable was hooked up to the ignitor as the last pre-firing step.

**B. FIRING SEQUENCE**

The video recorder was manually started before each firing. The firing sequence was started by executing the LabTech Notebook program. If the Malvern 2600 and the windowed motor were being used together, background measurements were taken before and after the motor firing to determine if window contamination occurred. The igniter was started by manually applying battery voltage to the nichrome wire embedded in the ignitor. The resulting current flow heated the nichrome wire and caused combustion of the $BKNO_3$, which in turn ignited the propellant in the motor. When the chamber pressure reached approximately 100 psig, a timer was started. After a desired

time delay, an external trigger was sent to the laser particle sizing system to commence data acquisition. The timing of this external trigger and the pressure-time trace were recorded by the LabTech Notebook program. After each successful firing, the video recorder was manually turned off and the AGEMA 870 IR Camera was secured after checking for sequence storage. Then the solenoid valves were shut to secure nitrogen gas flow. The motor was allowed to cool off and then disassembled and thoroughly cleaned in preparation for the next experiment.

Following the experiment, the optical data were saved automatically to the Malvern 2600. Then, the data collected by LabTech Notebook were manipulated to provide a pressure-time trace with data acquisition sequence markers superimposed. The data collected by the IR camera were used to examine the thermal image and the intensity of the plume radiation.

## IV. RESULTS AND DISCUSSIONS

### A. PRELIMINARY TESTS

Before the actual experiments, five check-out firings were executed to determine the optimum configuration and test sequence. First, a 2% aluminum, end-burning propellant grain was used together with a large igniter (to reduce ignition delays), the standard nozzle with 0.20 inches throat diameter and the windowed motor. Individual sonic chokes were used (0.030 inches and 0.020 inches diameter) to control the nitrogen flowrate to the windows. The total purge flowrate was 9% of the propellant mass flowrate. The upstream pressure to the sonic chokes was pre-set to 1400 psig to insure a constant flowrate with the expected chamber pressures of 400-600 psig. The chamber pressure exceeded 1500 psia during the first two firings, either due to the large igniter used or to cracks in the propellant.

Subsequent tests replaced the large igniter with a standard igniter and utilized one sonic choke (.030" diameter) to provide the window purge nitrogen. This resulted in obtaining a pressure of approximately 660 psia with relatively clean windows.

The last check-out test was conducted using the propellant with 5% aluminum and increased window purge flowrate

($d_{choke}$=0.035"). Another condition was then observed. The cold nitrogen flow into the window cavities apparently caused condensation on the windows. However, when the motor ignited the condensation disappeared.

After the check-out runs, the data runs were executed. There were three sets of experiments. Both the newly designed long and submerged nozzles were used with the small motor. The standard nozzle was used with the windowed motor. The Malvern 2600, the AGEMA 870 IR camera and the video camera were used for all of the experiments. The results of all the experiments are summarized in Table II.

## B. NOZZLE ENTRANCE PARTICLE SIZE DISTRIBUTION (EXPERIMENT 1)

The configuration used is shown Figure 4.1. The exhaust nozzle had a 45° converging half-angle and a throat diameter of 0.0242 inches. The distance from the propellant grain surface to the windows where the Malvern took data was 10.56 inches and the distance from there to the nozzle entrance was 0.32 inches. It was assumed that the particle size distribution measured at the entrance to this nozzle would be unchanged for the other nozzles employed.

An initial test firing resulted in a high pressure (998 psia), apparently due to nozzle throat deposits. For this reason a thin coating of an anti-siezing compound was applied to the converging section and the throat of the nozzle. Then two successful experiments were achieved using the same

configuration. The results of these runs were very consistent with each other (See Figs. 4.2, 4.3 and Table II). However, with small motors some test-to-test variations in the measured particle size distributions are expected due to the shedding of nozzle accumulations (observed to occur periodically in the video recordings) and to pieces of RTV inhibitor.

A bi-modal distribution was observed at the nozzle entrance, with most of the mass of particles in the mode centered at approximately 6 μm. The other mode occurred below the 2 μm resolution limit of the Malvern and contained less than 22% of the particulate mass. In these runs a very high obscuration was obtained (94-99%), which resulted from a very large number of very small particles. The high obscuration also affects the accuracy of the Malvern readings. The maximum $Al_2O_3$ particle diameter detected was 11.1 μm and $D_{32}$ was about 3.2 μm. However, the very high obscuration could mask the presence of a few number of large particles and the multiple scattering effects cause the measured $D_{32}$ to be smaller than that actually present. For these conditions, [Ref. 14], $D_{32actual} \approx 2 \times D_{32measured} \approx 6$ μm. With high obscuration the Malvern generally locates the modes correctly, but the percentage of mass in each mode may not be accurate. In a similar experiment Laredo, et al found $D_{32}$ to be 4.8 μm and a tri-modal distribution with modes at <2, 3 and 8 [Ref. 6]. They reported that only 1-5% of the mass was contained in particles <2 μm in diameter vs. the 12-13% noted in Table II.

## C. PARTICLE BEHAVIOR ACROSS STANDARD NOZZLE (EXPERIMENT 2)

The general set-up for this experiment is shown in Figure 4.4. The experiment was repeated five times. The results at the nozzle exit are shown in Table II and Figures 4.5-4.9. During these runs the windows were plugged with steel inserts and the window purge lines were capped. In the first run a low pressure (275 psia) was obtained, resulting in subsequent tests being made with an exhaust nozzle throat diameter of 0.209 inches. The residence time of the particles through the standard nozzle was approximately 0.06 msec. The nozzle exit pressure was under-expanded for all runs.

As expected, there was some test-to-test variation in pressure and measured particle size distributions due, apparently, to nozzle wall deposits/shedding and/or poor propellant bonding to the walls. Laser beam obscuration was not a problem in the plume, being almost always less than 50%. However, some beam steering was present. Beam steering deflects some of the centrally focused (unscattered) light from the pinhole in front of the central diode. The light scattered on the first few inner diode rings is dominated by this effect and is evidenced by a Gaussian intensity profile. The data in the first eight diode rings were "killed" to get rid of the beam steering. This resulted in a maximum detectable particle diameter of 78 μm (assuming that accuracy requires collecting all of the light in the first Airy diffraction ring).

The maximum size detected was 31 μm. It was found that the distribution was bi-modal or tri-modal. Typical modes were <2,3.5,20 μm. The low pressure and high pressure tests produced bi-modal distributions. The average $D_{32}$ was approximately 2.0 μm

Across the nozzle (experiment 1 to experiment 2 in Table II) it is observed that the percentage of mass contained in particles smaller than 2 μm increases significantly and larger modes are also produced. This shows that particles break up to produce very small particles through the nozzle, while at the same time the faster moving small particles collide with the slower moving large particles to produce even larger particles (collision coalescence). Both of these results are in agreement with earlier NPS data [Ref. 6] and the data of Traineau [Ref.9]. In a concurrent investigation using a PDPA [Ref. 11] $D_{max}$ was found to be 30 μm, in good agreement with the Malvern data.

Laredo, et al [Ref.6] also found under similar conditions that $D_{32}$ as 2.0 μm and the mass percent in particles less than 2 μm was approximately 35%. A typical distribution had modes at <2,4,13. These results are in general agreement with the results of this investigation.

It is not clear at this time whether the results obtained at higher pressure (e.g., more breakup and less collision coalescence) (experiment 2, run 5) are characteristic of

higher pressures or the result of increased accumulation of larger particles on the nozzle walls. Further data are needed.

### D. EFFECT OF NOZZLE RESIDENCE TIME (EXPERIMENT 3)

The small subscale motor was used with the long nozzle for this experiment. Thus, the nozzle residence time was almost doubled (0.127 ms vs 0.06 ms). Two firings were made with consistent results (See Table II and Figs. 4.10, 4.11). The increased consistency may have resulted from less nozzle wall collisions by large particles due to the decreased converging angle. Beam steering was again present as discussed above. The exit pressure was under-expanded.

Comparing the standard nozzle results to those with the increased residence time and approximately the same pressures (experiment 2-2,3 vs. experiment 3-1,2) it was found that $D_{32}$ decreased slightly, $D_{max}$ was unchanged, the mass percent in particles less than 2 μm greatly increased (from approximately 35% to 72%) and the modes of the tri-modal distributions were similar. These initial results imply that the increased nozzle residence time permits more particle breakup (time at critical Weber number [Ref. 7]) but does not change the collision coalescence process. Thus, it is expected that full-scale motors will have a larger percentage of mass in small particles than subscale motors, but the maximum sizes should be similar.

## E. EFFECT OF SUBMERGED NOZZLE (EXPERIMENT 4)

The subscale small motor was used with the submerged nozzle in this experiment. The results from these runs are shown in Table II and Figures 4.12-4.14.

In this experiment the slag accumulation around the submerged nozzle was examined. The propellant was weighed very precisely before each run. After the run the particles that accumulated above the submerged part of the nozzle were scrapped using a razor blade. The samples were cleaned by repeated ultrasonic mixing with acetone followed by eight hours of settling. Each sample was then weighed. For an assumed uniformly distributed particle distribution across the chamber diameter, 5.84 gm of $Al_2O_3$ would have been present above the submerged part of the nozzle. Only approximately 3% of this mass was actually collected. It is generally believed that only large (>100 μm) particles result in accumulation above the submerged nozzle because smaller particles can track the gas flow adequately to pass into the nozzle convergence [Ref. 4]. If it is assumed that only 100 μm particles were collected, there would have been approximately 216,000 present in the collected sample. The residue was transferred to SEM pedestals for examination (See Figs. 4.15,4.16). It was found that most particles were approximately 10-15 μm in diameter but that there were a small number of large $Al_2O_3$ particles (greater than 100 μm with a maximum of 140-150 μm). The small mass fraction of large particles could not be detected by the

Malvern at the nozzle entrance because of the very high obscuration from the very small particles. However, the small number of very large particles observed could represent a significant fraction of the collected mass.

These results imply that particles with sizes significantly less than 100 μm can collect above submerged nozzles. Together with the Malvern measurements made at the nozzle entrance these results also indicate that most of the particle mass at the nozzle entrance is not contained in large particles, in agreement with Reference 6.

## F. NOZZLE EFFECTS ON PLUME IR SIGNATURE

The thermal image from each test was recorded to determine if any significant changes in particle size would have any effect on plume IR signature. Since none of the tests resulted in large changes in the plume particle size distribution, no plume radiation changes were expected. The total radiation in the 3.5-5 μm range from each test is shown in Figure 4.17 and confirmed the expected result.

## V. CONCLUSIONS AND RECOMMENDATIONS

There were two questions before beginning this investigation. Are particle size data obtained with subscale motors applicable to full-scale motors? Does slag mass accumulation behind submerged nozzles correlate with the presence of large (>100 μm) particles?

It was found that small motors with rapidly converging nozzles have a tendency for the throat to plug and for particles to collide, accumulate and shed from the converging wall. This also can result in throat-clogging with test-to-test variations in the chamber pressure, which affected the measured size distribution of the particles in the plume.

The results were in good agreement with the data of Traineau [Ref. 9] and Laredo [Ref. 6]. Both particle breakup and collision coalescence occurred across the exhaust nozzle, with a significant increase in the mass fraction of small (<2 μm) particles.

Although particles as large as 140 μm were present at the nozzle entrance, most particulate mass was contained in much smaller particles. This was evidenced by Malvern measurements, SEM photos of collected residue, high obscurations of the laser beam and the weight of collected residue above the submerged nozzle. Since many particles leaving the propellant surface are known to be quite large, the results suggest that

a currently unknown mechanism (such as periodic shedding of the oxide lobe) results in particle breakup within the low Mach number environment in the chamber.

Increasing the nozzle residence time enhanced particle breakup (apparently through increased time at critical Weber number conditions) but did not alter the maximum plume particle size. Thus, full-scale motors are expected to have a higher percentage of mass in particles less than 2 $\mu$m than subscale motors but with similar diameters of the largest particles.

The mass that collects above submerged nozzles includes particles with diameters significantly less than 100 $\mu$m, but most of the collected mass (which was small) could have resulted from large particles. The significant amount of $Al_2O_3$ mass accumulation reported for large motors may be occurring in part from surface movement of molten $Al_2O_3$ rather than just the trajectory behavior of large particles.

The following recommendations are made for further experimentation in this area of research:

(1)Data be taken using the PDPA to more accurately determine the mass percent contained in large particles.

(2)A technique be developed to provide more test-to-test repeatability for subscale motors.

## APPENDIX A

## TABLES

TABLE I

PROPELLANT COMPOSITION

| INGREDIENTS | PERCENTAGES |
|---|---|
| AP (200 microns) | 45.70% |
| AP (25 microns) | 24.61% |
| GAP (200-1) | 14.67% |
| TEGDN (AK-17E) | 8.49% |
| Aluminum (C003) | 4.68% |
| Others | 1.84% |

Burning rate (in/sec) = $0.0437 * P_c^{0.660}$

where $P_c$ is in psia

TABLE II

THE RESULTS OF THE EXPERIMENTS

| CONF. | $P_e$ (psia) | $d_{th}$ (inch.) | $P_{cmax}$ (psia) | $P_{chalvern}$ (psia) | $D_{32}$ (μm) | $D_{43}$ (μm) | $D_{max}$ (μm) | Mod/% | %<2 |
|---|---|---|---|---|---|---|---|---|---|
| Exp 1 Run 1 | 22 | .242 | 372 | 305 | 3.1 | 4.6 | 11.1 | <2/21, 6/79 | 13 |
| Exp 1 Run 2 | 25 | .242 | 413 | 322 | 3.4 | 5.0 | 8.9 | <2/22, 6/78 | 12 |
| Exp 2 Run 1 | 16 | .242 | 275 | 253 | 1.5 | 3.5 | 14 | <2/63, 7/37 | 56 |
| Exp 2 Run 2 | 26 | .209 | 439 | 380 | 2.6 | 7.5 | 31 | <2/26, 3.7/36, 9/7,22/31 | 20 |
| Exp 2 Run 3 | 28 | .209 | 476 | 440 | 1.7 | 4.7 | 25 | <2/48, 3.3/38, 19/14 | 42 |
| Exp 2 Run 4 | 35 | .209 | 580 | 511 | 1.9 | 4.5 | 28 | <2/33, 3.3/57, 25/10 | 33 |
| Exp 2 Run 5 | 47 | .209 | 779 | 762 | 1.1 | 1.4 | 6.7 | <2/90, 3.6/10 | 79 |
| Exp 3 Run 1 | 26 | .200 | 399 | 359 | 1.3 | 4.7 | 28.4 | <2/72, 9/18,26/10 | 72 |
| Exp 3 Run 2 | 27 | .200 | 419 | 375 | 1.3 | 4.7 | 28.4 | <2/74, 9/15,22/11 | 72 |
| Exp 4 Run 1 | 24 | .200 | 543 | 458 | 1.3 | 2.9 | 30.6 | <2/90, 9/8,26/8 | 63 |
| Exp 4 Run 2 | 25 | .200 | 561 | 484 | 1.8 | 4.6 | 26.4 | <2/39, 3.8/47, 19/14 | 39 |
| Exp 4 Run 3 | 31 | .200 | 701 | 657 | 1.5 | 5.8 | 30.6 | <2/60, 3.8/23, 26/10 | 53 |

## APPENDIX B

## FIGURES

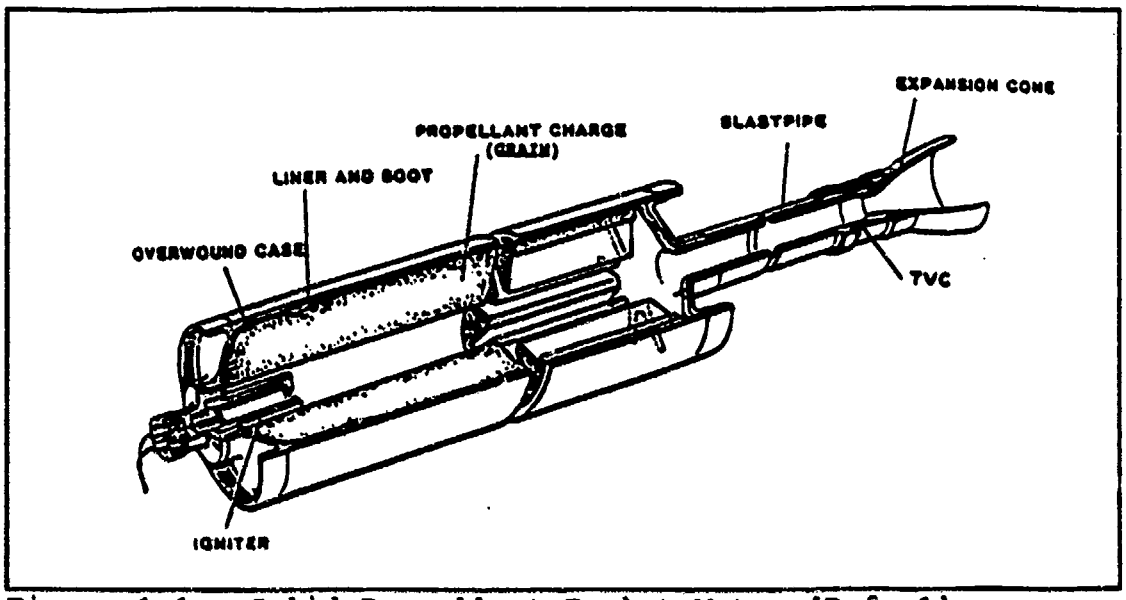


Figure 1.1 Solid Propellant Rocket Motor [Ref. 1]

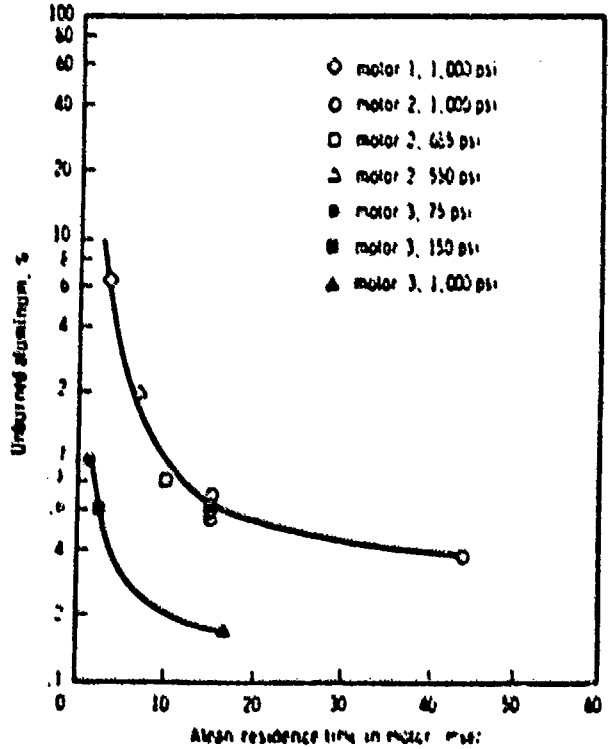


Figure 1.2 Effect of $t_{res}$ on Aluminum Combustion [Ref. 5]

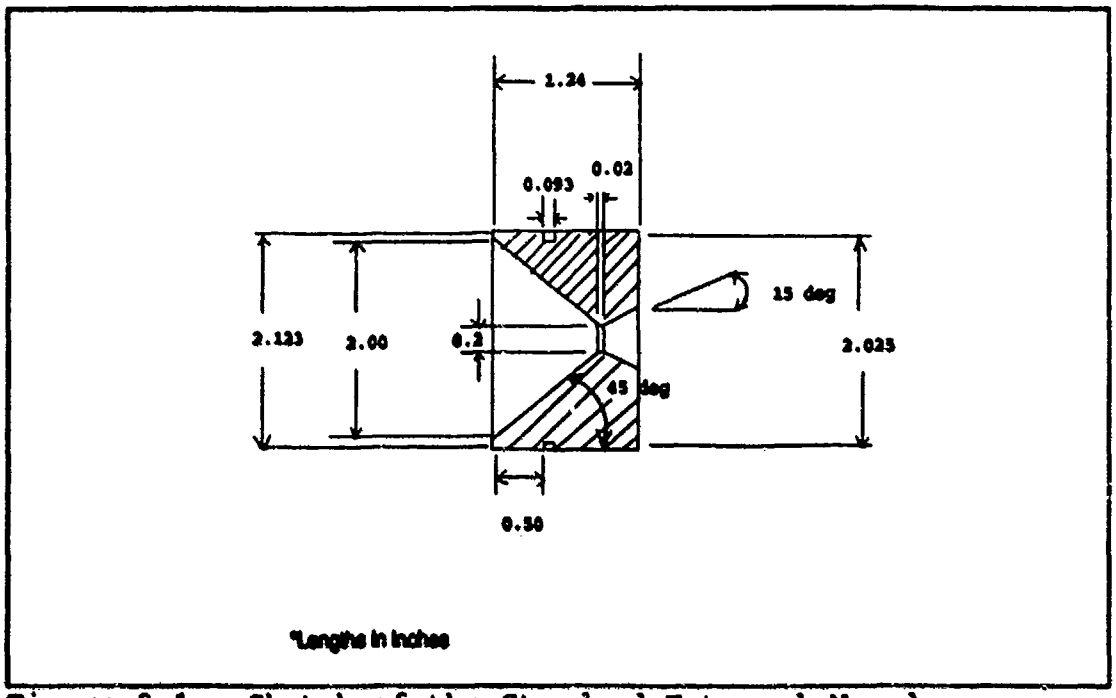


Figure 2.1 Sketch of the Standard External Nozzle

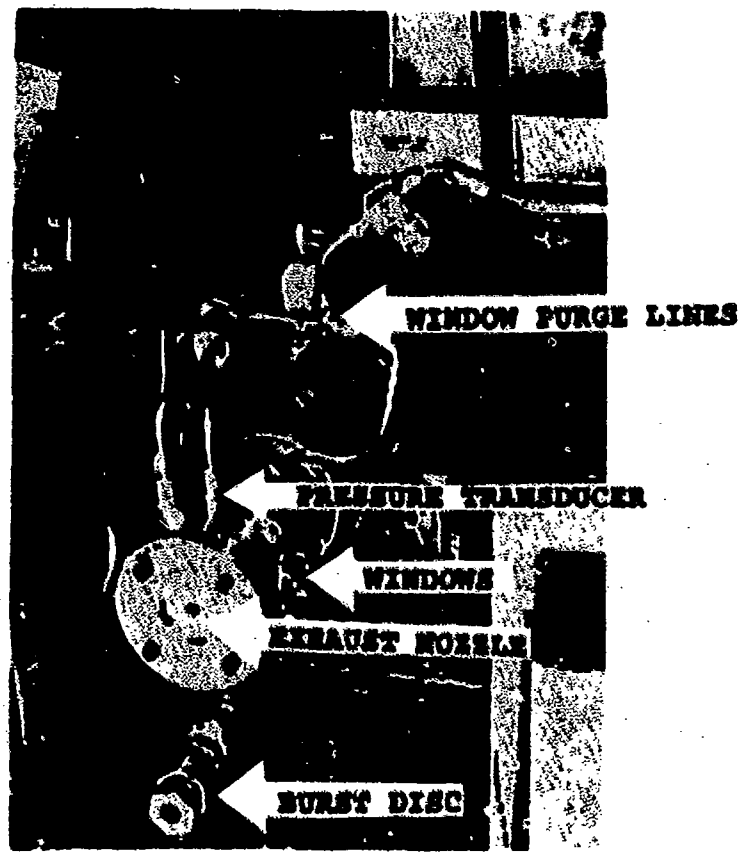


Figure 2.2 Subscale Windowed Motor

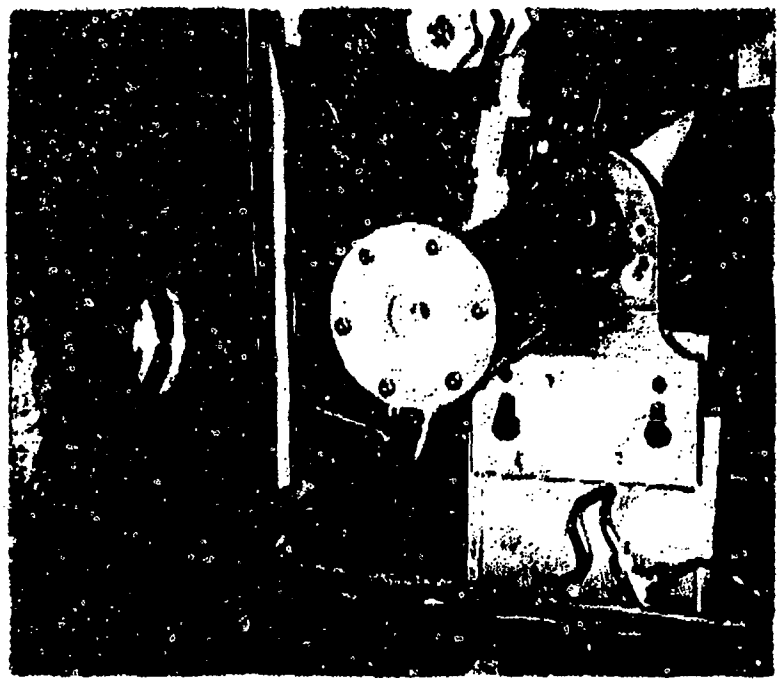

Figure 2.3 Subscale Small Motor

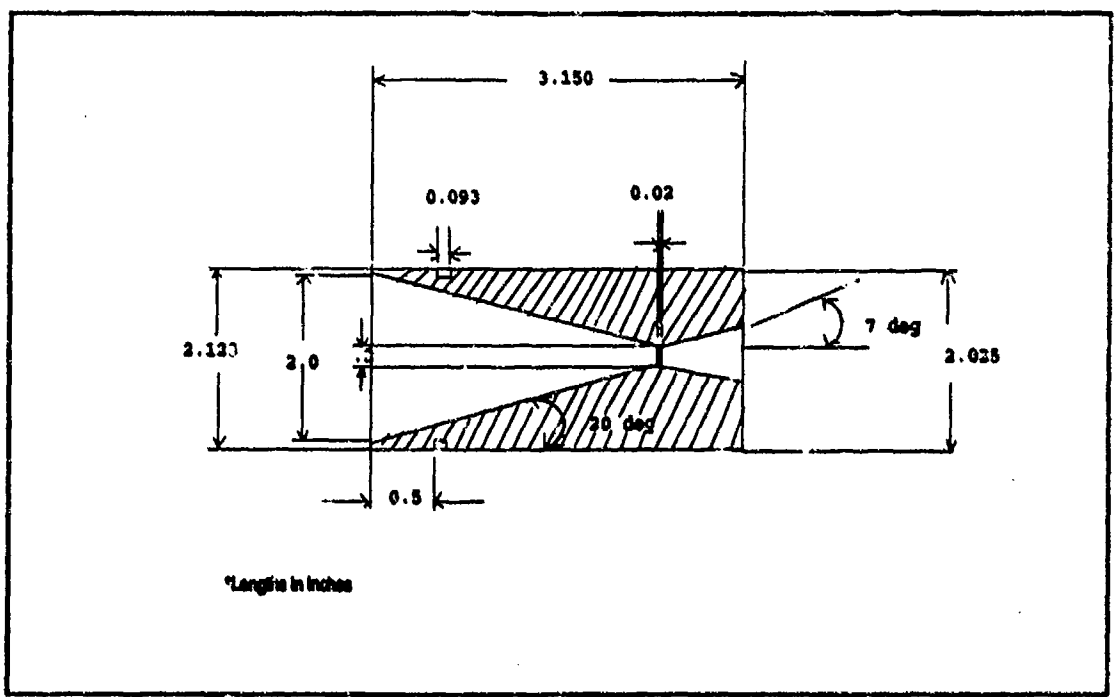


Figure 2.4 Sketch of the External Long Nozzle

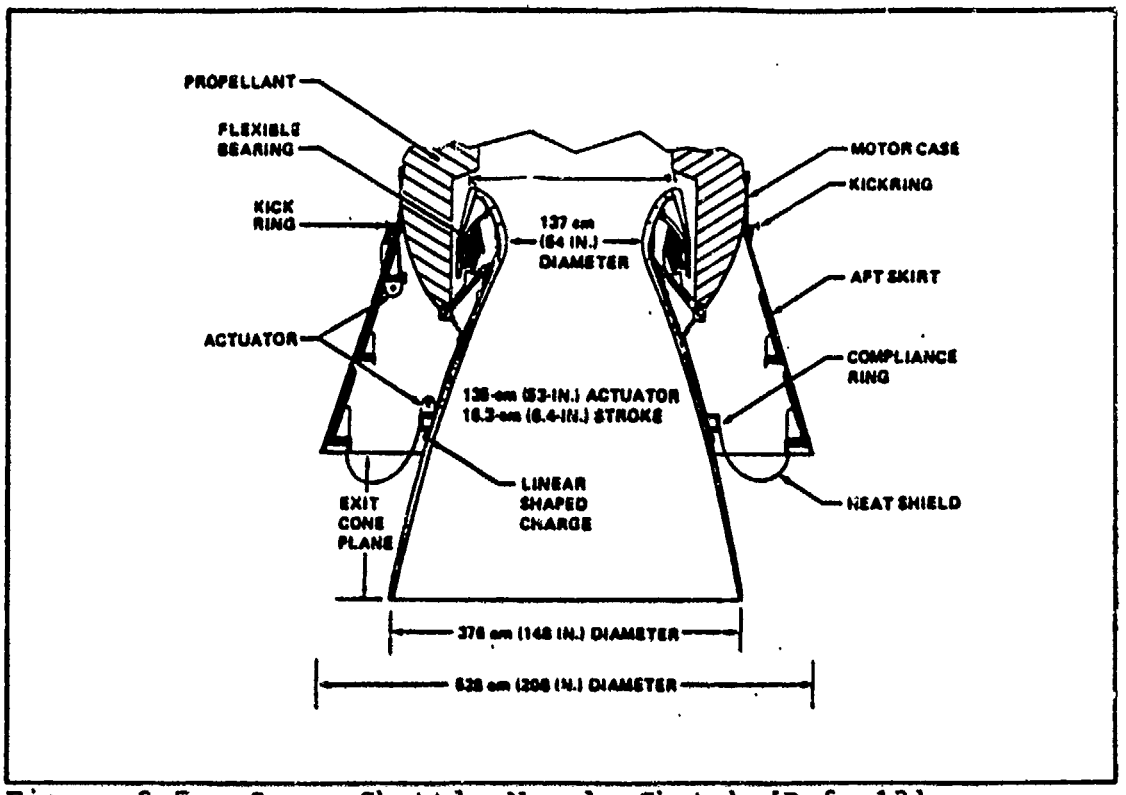


Figure 2.5 Space Shuttle Nozzle Sketch [Ref. 13]

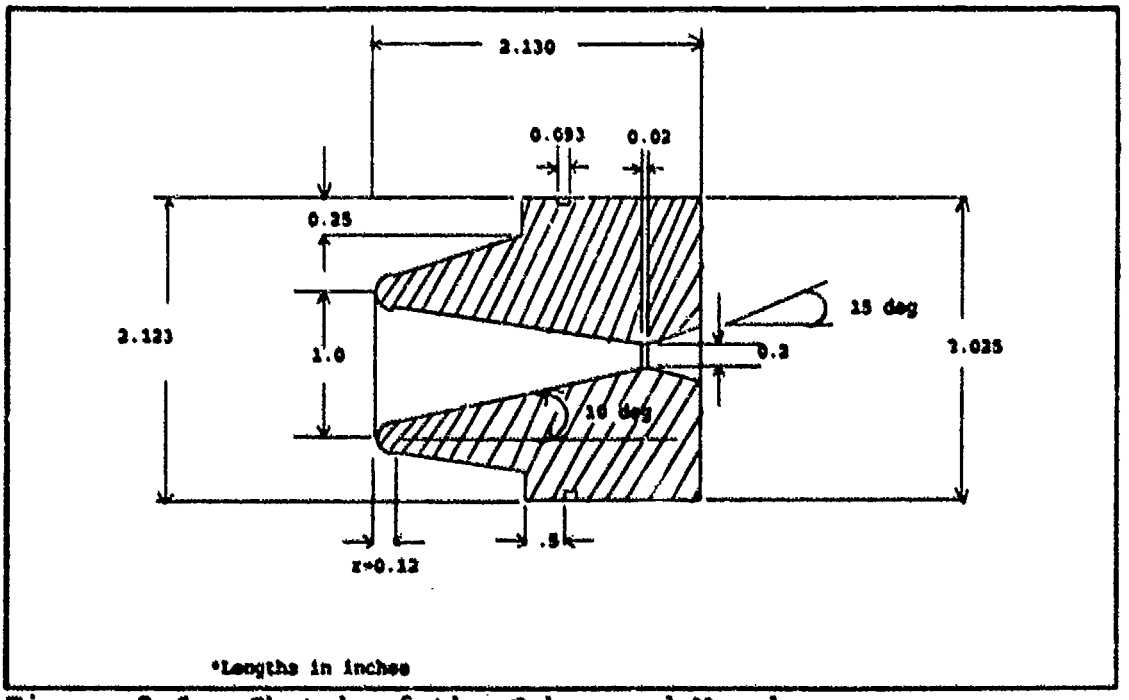


Figure 2.6 Sketch of the Submerged Nozzle

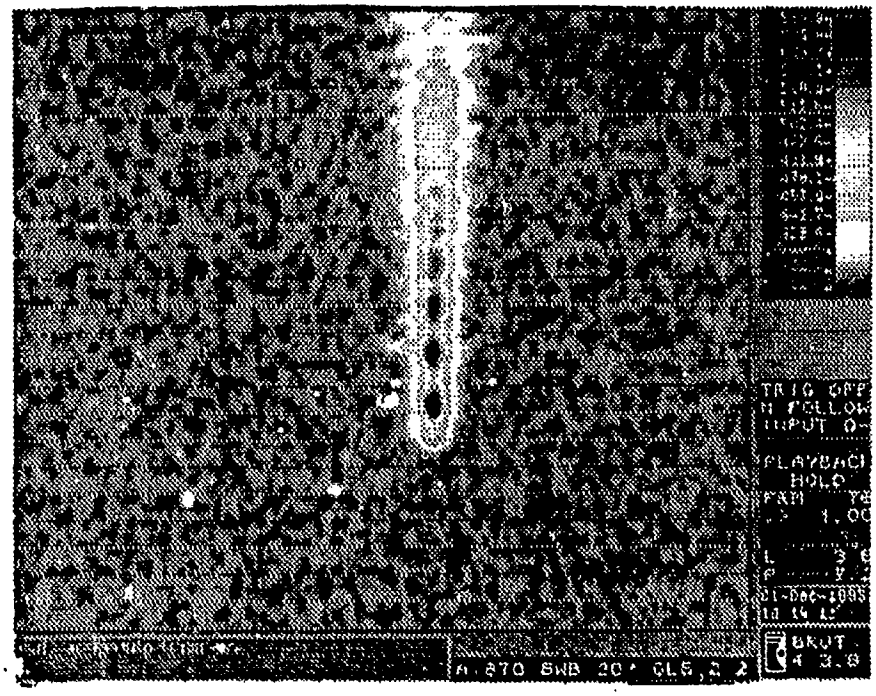

Figure 2.7 Example of AGEMA Data

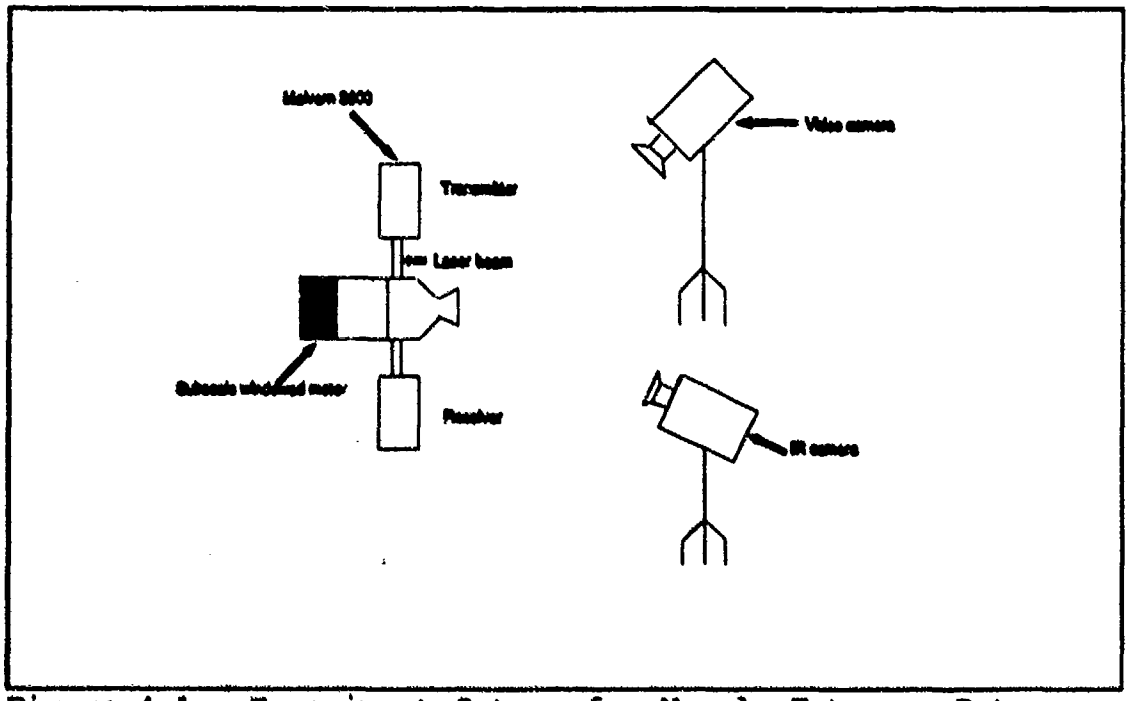


Figure 4.1 Experiment Set-up for Nozzle Entrance Data

| Upper | in | Lower | Under | Upper | in | Lower | Under | Upper | in | Lower | Under | Span 0.93 |
|---|---|---|---|---|---|---|---|---|---|---|---|---|
| | | | | 57.7 | 0.0 | 49.8 | 100 | 9.82 | 0.0 | 8.47 | 99.9 | |
| | | | | 49.8 | 0.0 | 43.0 | 100 | 8.47 | 3.4 | 7.30 | 96.5 | D[4,3] 4.55µm |
| | | | | 43.0 | 0.0 | 37.0 | 100 | 7.30 | 8.4 | 6.30 | 88.1 | |
| | | | | 37.0 | 0.0 | 32.0 | 100 | 6.30 | 26.0 | 5.43 | 62.1 | |
| 188 | 0.0 | 162 | 100 | 32.0 | 0.0 | 27.5 | 100 | 5.43 | 24.8 | 4.68 | 37.3 | D[3,2] 3.10µm |
| 162 | 0.0 | 140 | 100 | 27.5 | 0.0 | 23.8 | 100 | 4.68 | 7.7 | 4.05 | 29.6 | |
| 140 | 0.0 | 121 | 100 | 23.8 | 0.0 | 20.5 | 100 | 4.05 | 4.6 | 3.48 | 25.0 | |
| 121 | 0.0 | 104 | 100 | 20.5 | 0.0 | 17.7 | 100 | 3.48 | 1.9 | 3.02 | 23.1 | D[v,0.9] 6.47µm |
| 104 | 0.0 | 89.8 | 100 | 17.7 | 0.0 | 15.3 | 100 | 3.02 | 2.2 | 2.60 | 20.9 | |
| 89.8 | 0.0 | 77.5 | 100 | 15.3 | 0.0 | 13.2 | 100 | 2.60 | 3.6 | 2.23 | 17.3 | |
| 77.5 | 0.0 | 66.8 | 100 | 13.2 | 0.0 | 11.4 | 100 | 2.23 | 4.2 | 1.93 | 13.1 | D[v,0.1] 1.71µm |
| 66.8 | 0.0 | 57.7 | 100 | 11.4 | 0.1 | 9.82 | 99.9 | 1.93 | 13.1 | 0.50 | 0.0 | |
| Source = Data:27octby | | | | Beam length = 50.0 mm | | | | Model indp | | | | D[v,0.5] 5.12µm |
| Record No. = 1 | | | | Log. Diff. = 5.075 | | | | | | | | |
| Focal length = 100 mm | | | | Obscuration = 0.9900 | | | | Volume Conc. = 0.0095% | | | | |
| Presentation = pia | | | | Volume distribution | | | | Sp.S.A 1.9344 m²/cc. | | | | Shape OFF |

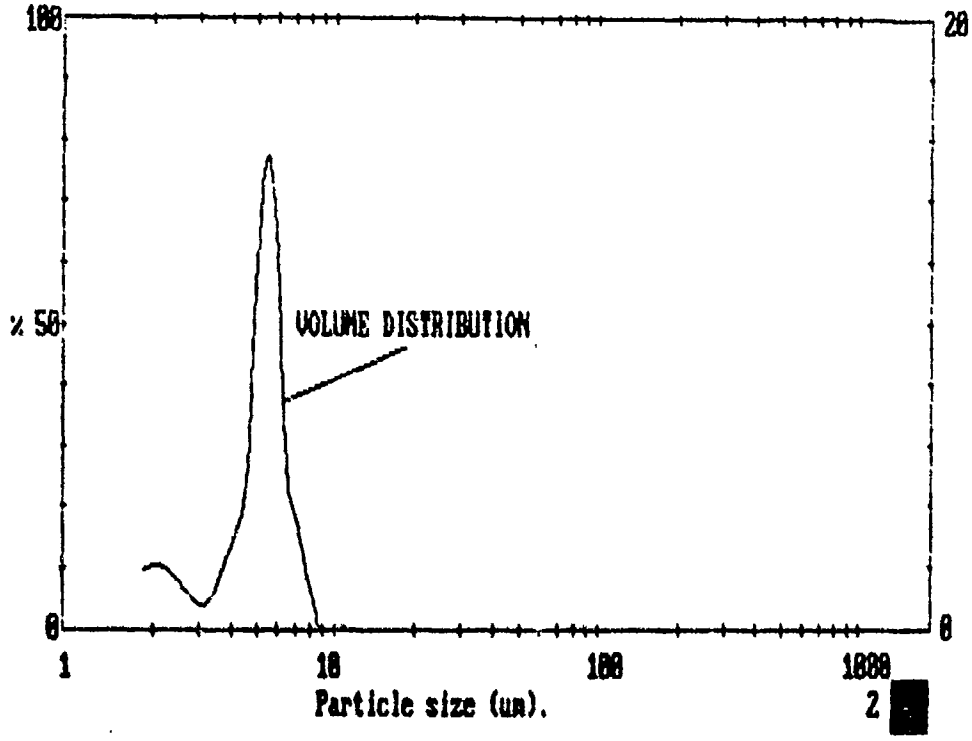


Figure 4.2 Malvern Results of Experiment 1, Run 1

| Upper | in | Lower | Under | Upper | in | Lower | Under | Upper | in | Lower | Under | Span 0.89 |
|---|---|---|---|---|---|---|---|---|---|---|---|---|
| | | | | 57.7 | 0.0 | 49.8 | 100 | 9.82 | 0.0 | 8.47 | 100 | |
| | | | | 49.8 | 0.0 | 43.0 | 100 | 8.47 | 3.5 | 7.30 | 96.5 | D[4,3] 5.04µm |
| | | | | 43.0 | 0.0 | 37.0 | 100 | 7.30 | 20.6 | 6.30 | 75.9 | |
| | | | | 37.0 | 0.0 | 32.0 | 100 | 6.30 | 34.3 | 5.43 | 41.6 | |
| 188 | 0.0 | 162 | 100 | 32.0 | 0.0 | 27.5 | 100 | 5.43 | 18.5 | 4.68 | 23.1 | D[3,2] 3.42µm |
| 162 | 0.0 | 140 | 100 | 27.5 | 0.0 | 23.8 | 100 | 4.68 | 1.0 | 4.05 | 22.1 | |
| 140 | 0.0 | 121 | 100 | 23.8 | 0.0 | 20.5 | 100 | 4.05 | 0.5 | 3.48 | 21.7 | |
| 121 | 0.0 | 104 | 100 | 20.5 | 0.0 | 17.7 | 100 | 3.48 | 1.4 | 3.02 | 20.3 | D[v,0.9] 6.82µm |
| 104 | 0.0 | 89.8 | 100 | 17.7 | 0.0 | 15.3 | 100 | 3.02 | 2.0 | 2.60 | 18.3 | |
| 89.8 | 0.0 | 77.5 | 100 | 15.3 | 0.0 | 13.2 | 100 | 2.60 | 3.2 | 2.23 | 15.2 | |
| 77.5 | 0.0 | 66.8 | 100 | 13.2 | 0.0 | 11.4 | 100 | 2.23 | 3.7 | 1.93 | 11.5 | D[v,0.1] 1.82µm |
| 66.8 | 0.0 | 57.7 | 100 | 11.4 | 0.0 | 9.82 | 100 | 1.93 | 11.5 | 0.50 | 0.0 | |
| Source = Data:26octby | | | | Beam length = 50.0 mm | | | | Model indp | | | | D[v,0.5] 5.64µm |
| Record No. = 1 | | | | Log. Diff. = 5.260 | | | | | | | | |
| Focal length = 100 mm | | | | Obscuration = 0.9437 | | | | Volume Conc. = 0.0066% | | | | |
| Presentation = pia | | | | Volume distribution | | | | Sp.S.A 1.7554 m²/cc. | | | | Shape OFF |

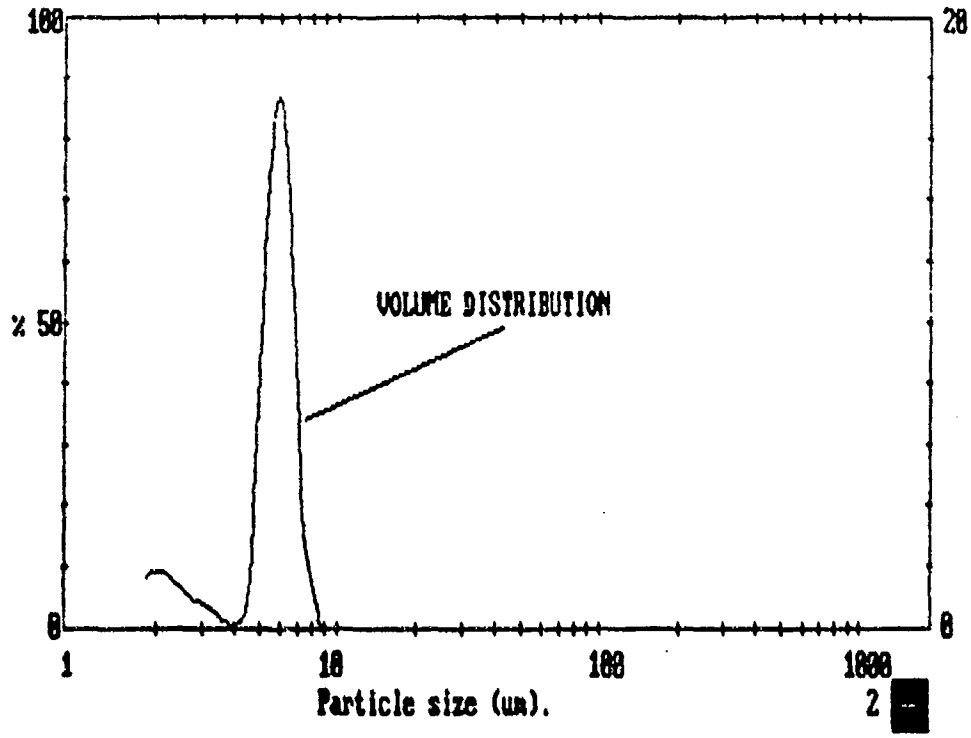


Figure 4.3 Malvern Results of Experiment 1, Run 2

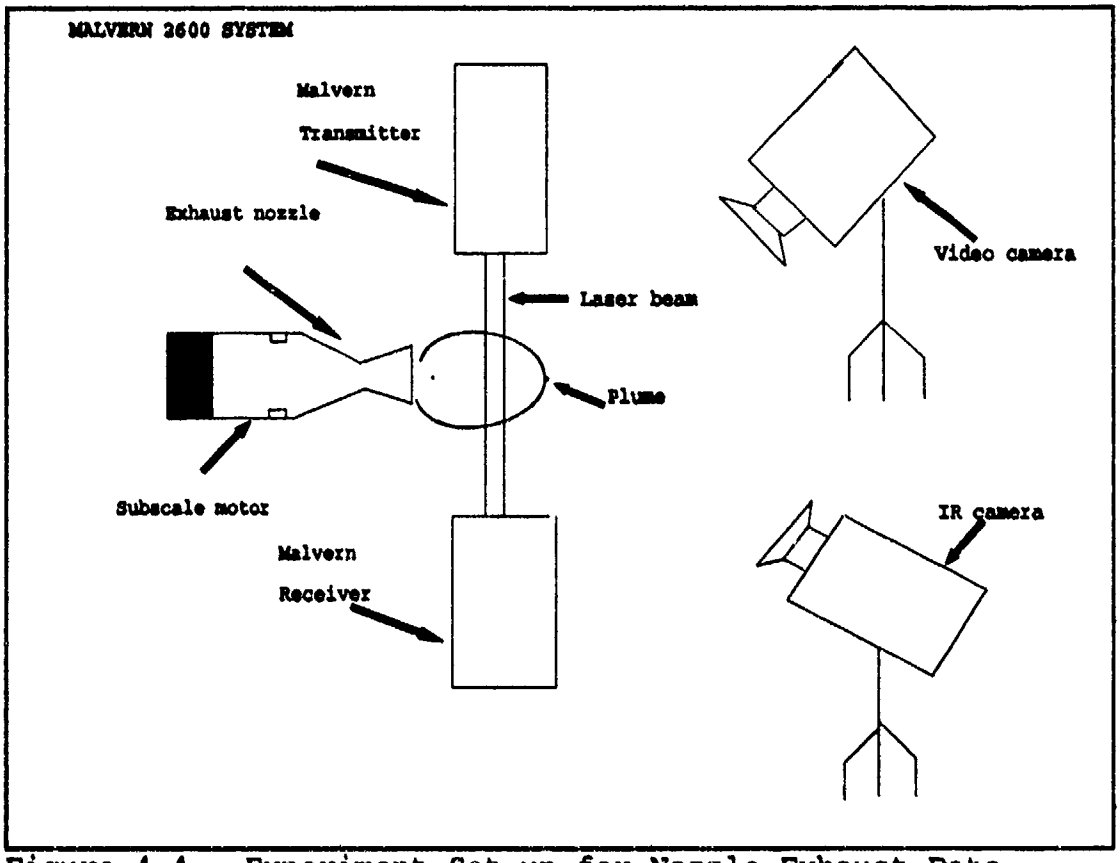


Figure 4.4 Experiment Set-up for Nozzle Exhaust Data

| Upper | in | Lower | Under | Upper | in | Lower | Under | Upper | in | Lower | Under | Span 4.32 |
|---|---|---|---|---|---|---|---|---|---|---|---|---|
| | | | | 57.7 | 0.0 | 49.8 | 100 | 9.82 | 3.5 | 8.47 | 91.4 | |
| | | | | 49.8 | 0.0 | 43.0 | 100 | 8.47 | 8.1 | 7.30 | 83.3 | D[4,3] 3.46µm |
| | | | | 43.0 | 0.0 | 37.0 | 100 | 7.30 | 10.5 | 6.30 | 72.8 | |
| | | | | 37.0 | 0.0 | 32.0 | 100 | 6.30 | 5.8 | 5.43 | 67.1 | |
| 188 | 0.0 | 162 | 100 | 32.0 | 0.0 | 27.5 | 100 | 5.43 | 1.9 | 4.68 | 65.1 | D[3,2] 1.53µm |
| 162 | 0.0 | 140 | 100 | 27.5 | 0.0 | 23.8 | 100 | 4.68 | 1.2 | 4.05 | 63.9 | |
| 140 | 0.0 | 121 | 100 | 23.8 | 0.0 | 20.5 | 100 | 4.05 | 0.7 | 3.48 | 63.2 | |
| 121 | 0.0 | 104 | 100 | 20.5 | 0.0 | 17.7 | 100 | 3.48 | 0.0 | 3.02 | 63.2 | D[v,0.9] 8.18µm |
| 104 | 0.0 | 89.8 | 100 | 17.7 | 0.0 | 15.3 | 100 | 3.02 | 0.0 | 2.60 | 63.2 | |
| 89.8 | 0.0 | 77.5 | 100 | 15.3 | 0.0 | 13.2 | 100 | 2.60 | 2.0 | 2.23 | 61.2 | |
| 77.5 | 0.0 | 66.8 | 100 | 13.2 | 1.9 | 11.4 | 98.1 | 2.23 | 5.4 | 1.93 | 55.8 | D[v,0.1] 0.78µm |
| 66.8 | 0.0 | 57.7 | 100 | 11.4 | 3.2 | 9.82 | 94.9 | 1.93 | 55.8 | 0.50 | 0.0 | |
| Source = Data:Input | | | | Beam length = 50.0 mm | | | | Model indp [ 4, 0 ] | | | | D[v,0.5] 1.71um |
| Focal length = 100 mm | | | | Log. Diff. = 2.929 | | | | | | | | |
| Presentation = pia | | | | Obscuration = 0.5038 | | | | Volume Conc. = 0.0007% | | | | Shape OFF |
| | | | | Volume distribution | | | | Sp.S.A 3.9267 m²/cc. | | | | |

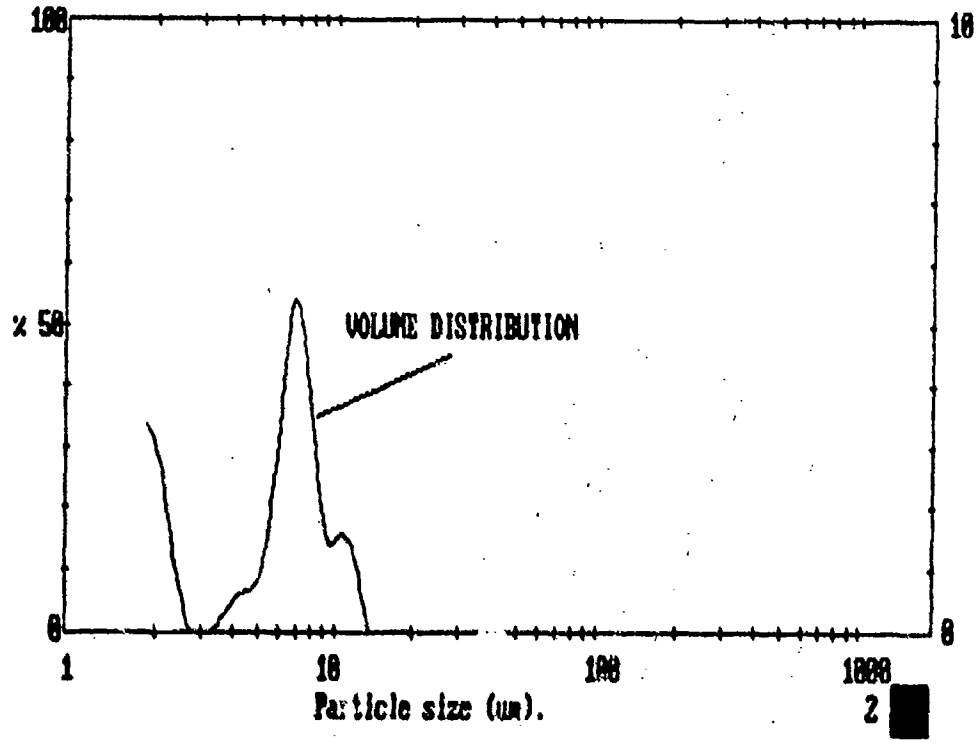


Figure 4.5 Malvern Results of Experiment 2, Run 1

| Upper | in | Lower | Under | Upper | in | Lower | Under | Upper | in | Lower | Under | Span 5.66 |
|---|---|---|---|---|---|---|---|---|---|---|---|---|
| | | | | 57.7 | 0.0 | 49.8 | 100 | 9.82 | 2.4 | 8.47 | 72.9 | |
| | | | | 49.8 | 0.0 | 43.0 | 100 | 8.47 | 2.2 | 7.30 | 70.7 | D[4,3] 7.45µm |
| | | | | 43.0 | 0.0 | 37.0 | 100 | 7.30 | 1.9 | 6.30 | 68.8 | |
| | | | | 37.0 | 0.0 | 32.0 | 100 | 6.30 | 2.0 | 5.43 | 66.8 | |
| 188 | 0.0 | 162 | 100 | 32.0 | 0.2 | 27.5 | 99.8 | 5.43 | 3.8 | 4.68 | 63.1 | D[3,2] 2.64µm |
| 162 | 0.0 | 140 | 100 | 27.5 | 4.9 | 23.8 | 94.9 | 4.68 | 6.5 | 4.05 | 56.6 | |
| 140 | 0.0 | 121 | 100 | 23.8 | 8.5 | 20.5 | 86.4 | 4.05 | 8.4 | 3.48 | 48.2 | |
| 121 | 0.0 | 104 | 100 | 20.5 | 7.1 | 17.7 | 79.3 | 3.48 | 8.1 | 3.02 | 40.1 | D[v,0.9] 21.79µm |
| 104 | 0.0 | 89.8 | 100 | 17.7 | 1.7 | 15.3 | 77.7 | 3.02 | 7.3 | 2.60 | 32.9 | |
| 89.8 | 0.0 | 77.5 | 100 | 15.3 | 0.0 | 13.2 | 77.7 | 2.60 | 7.0 | 2.23 | 25.9 | |
| 77.5 | 0.0 | 66.8 | 100 | 13.2 | 0.5 | 11.4 | 77.1 | 2.23 | 6.3 | 1.93 | 19.6 | D[v,0.1] 1.44µm |
| 66.8 | 0.0 | 57.7 | 100 | 11.4 | 1.9 | 9.82 | 75.3 | 1.93 | 19.6 | 0.50 | 0.0 | |
| Source = Data:Input | | | | Beam length = 50.0 mm | | | | Model indp [ 4, 0 ] | | | | D[v,0.5] 3.59µm |
| Focal length = 100 mm | | | | Log. Diff. = 3.345 | | | | | | | | |
| Presentation = pia | | | | Obscuration = 0.4780 | | | | Volume Conc. = 0.0011% | | | | |
| | | | | Volume distribution | | | | Sp.S.A 2.2720 m²/cc. | | | | Shape OFF |

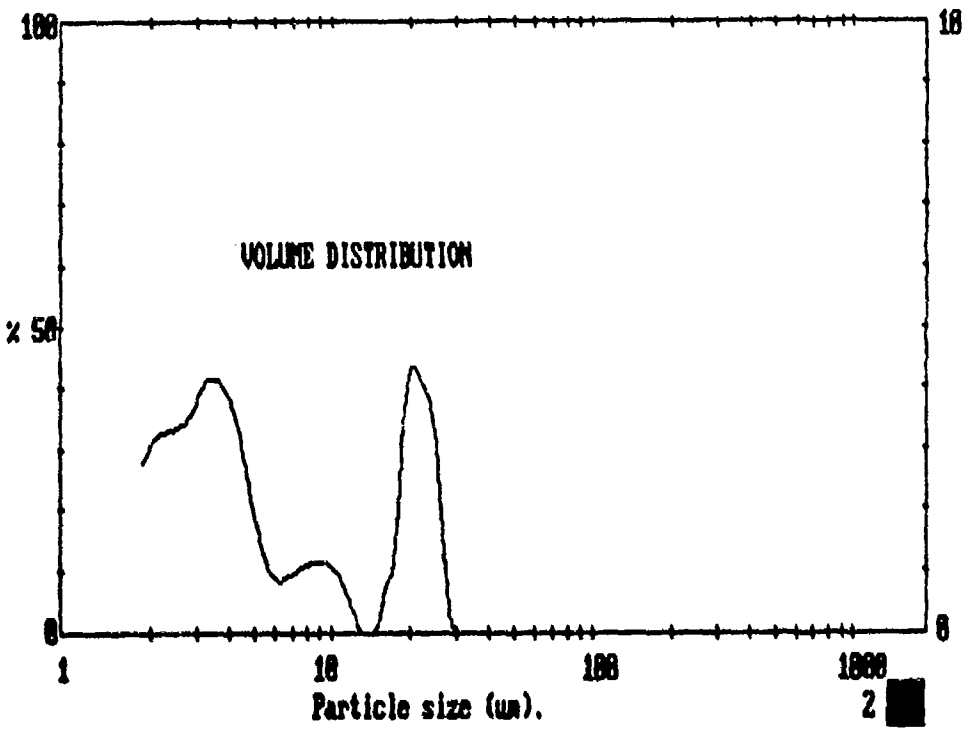


Figure 4.6 Malvern Results of Experiment 2, Run 2

| Upper | in | Lower | Under | Upper | in | Lower | Under | Upper | in | Lower | Under | Span 7.35 |
|---|---|---|---|---|---|---|---|---|---|---|---|---|
| | | | | 57.7 | 0.0 | 49.8 | 100 | 9.82 | 0.0 | 8.47 | 85.6 | |
| | | | | 49.8 | 0.0 | 43.0 | 100 | 8.47 | 0.0 | 7.30 | 85.6 | D[4,3] 4.65µm |
| | | | | 43.0 | 0.0 | 37.0 | 100 | 7.30 | 0.1 | 6.30 | 85.5 | |
| | | | | 37.0 | 0.0 | 32.0 | 100 | 6.30 | 0.3 | 5.43 | 85.2 | |
| 188 | 0.0 | 162 | 100 | 32.0 | 0.0 | 27.5 | 100 | 5.43 | 2.0 | 4.68 | 83.2 | D[3,2] 1.73µm |
| 162 | 0.0 | 140 | 100 | 27.5 | 0.0 | 23.8 | 100 | 4.68 | 5.3 | 4.05 | 77.9 | |
| 140 | 0.0 | 121 | 100 | 23.8 | 3.9 | 20.5 | 96.1 | 4.05 | 9.9 | 3.48 | 68.0 | |
| 121 | 0.0 | 104 | 100 | 20.5 | 8.2 | 17.7 | 87.9 | 3.48 | 10.0 | 3.02 | 58.0 | D[v,0.9] 18.46µm |
| 104 | 0.0 | 89.8 | 100 | 17.7 | 2.2 | 15.3 | 85.6 | 3.02 | 5.6 | 2.60 | 52.4 | |
| 89.8 | 0.0 | 77.5 | 100 | 15.3 | 0.0 | 13.2 | 85.6 | 2.60 | 4.5 | 2.23 | 47.9 | |
| 77.5 | 0.0 | 66.8 | 100 | 13.2 | 0.0 | 11.4 | 85.6 | 2.23 | 5.6 | 1.93 | 42.3 | D[v,0.1] 0.87µm |
| 66.8 | 0.0 | 57.7 | 100 | 11.4 | 0.0 | 9.82 | 85.6 | 1.93 | 42.3 | 0.50 | 0.0 | |
| Source = Data:Input | | | | Beam length = 50.0 mm | | | | Model indp [ 4, 0 ] | | | | D[v,0.5] 2.39µm |
| | | | | Log. Diff. = 3.785 | | | | | | | | |
| Focal length = 100 mm | | | | Obscuration = 0.4022 | | | | Volume Conc. = 0.0006% | | | | |
| Presentation = pia | | | | Volume distribution | | | | Sp.S.A 3.4644 m²/cc. | | | | Shape OFF |

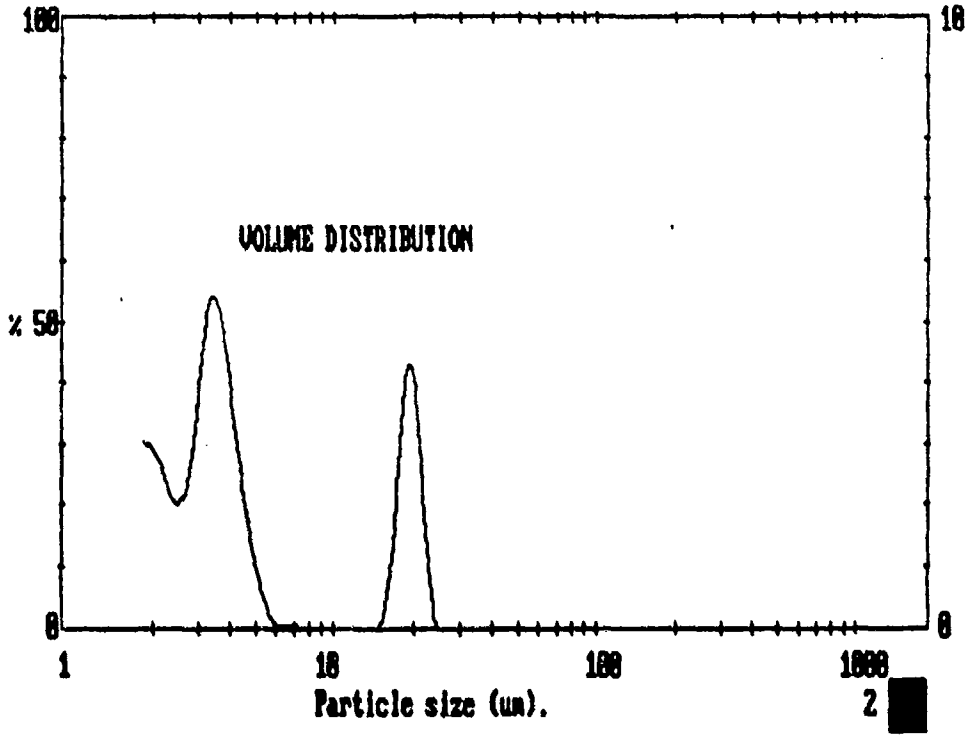


Figure 4.7 Malvern Results of Experiment 2, Run 3

| Upper | in | Lower | Under | Upper | in | Lower | Under | Upper | in | Lower | Under | Span 7.18 |
|---|---|---|---|---|---|---|---|---|---|---|---|---|
| | | | | 57.7 | 0.0 | 49.8 | 100 | 9.82 | 0.0 | 8.47 | 89.9 | |
| | | | | 49.8 | 0.0 | 43.0 | 100 | 8.47 | 0.0 | 7.30 | 89.9 | D[4,3] 4.47µm |
| | | | | 43.0 | 0.0 | 37.0 | 100 | 7.30 | 0.0 | 6.30 | 89.9 | |
| | | | | 37.0 | 0.0 | 32.0 | 100 | 6.30 | 0.0 | 5.43 | 89.9 | |
| 188 | 0.0 | 162 | 100 | 32.0 | 0.2 | 27.5 | 99.8 | 5.43 | 0.0 | 4.68 | 89.9 | D[3,2] 1.87µm |
| 162 | 0.0 | 140 | 100 | 27.5 | 5.4 | 23.8 | 94.4 | 4.68 | 0.3 | 4.05 | 89.6 | |
| 140 | 0.0 | 121 | 100 | 23.8 | 4.5 | 20.5 | 89.9 | 4.05 | 8.1 | 3.48 | 81.5 | |
| 121 | 0.0 | 104 | 100 | 20.5 | 0.0 | 17.7 | 89.9 | 3.48 | 20.7 | 3.02 | 60.9 | D[v,0.9] 20.57µm |
| 104 | 0.0 | 89.8 | 100 | 17.7 | 0.0 | 15.3 | 89.9 | 3.02 | 14.7 | 2.60 | 46.2 | |
| 89.8 | 0.0 | 77.5 | 100 | 15.3 | 0.0 | 13.2 | 89.9 | 2.60 | 8.2 | 2.23 | 38.0 | |
| 77.5 | 0.0 | 66.8 | 100 | 13.2 | 0.0 | 11.4 | 89.9 | 2.23 | 5.5 | 1.93 | 32.5 | D[v,0.1] 0.98µm |
| 66.8 | 0.0 | 57.7 | 100 | 11.4 | 0.0 | 9.82 | 89.9 | 1.93 | 32.5 | 0.50 | 0.0 | |
| Source = Data:Input<br>Focal length = 100 mm<br>Presentation = pia | | | | Beam length = 50.0 mm<br>Lg. Diff. = 3.900<br>Obscuration = 0.4928<br>Volume distribution | | | | Model indp [ 4, 0 ]<br>Volume Conc. = 0.0008%<br>Sp.S.A 3.2027 m²/cc. | | | | D[v,0.5] 2.73µm<br>Shape OFF |

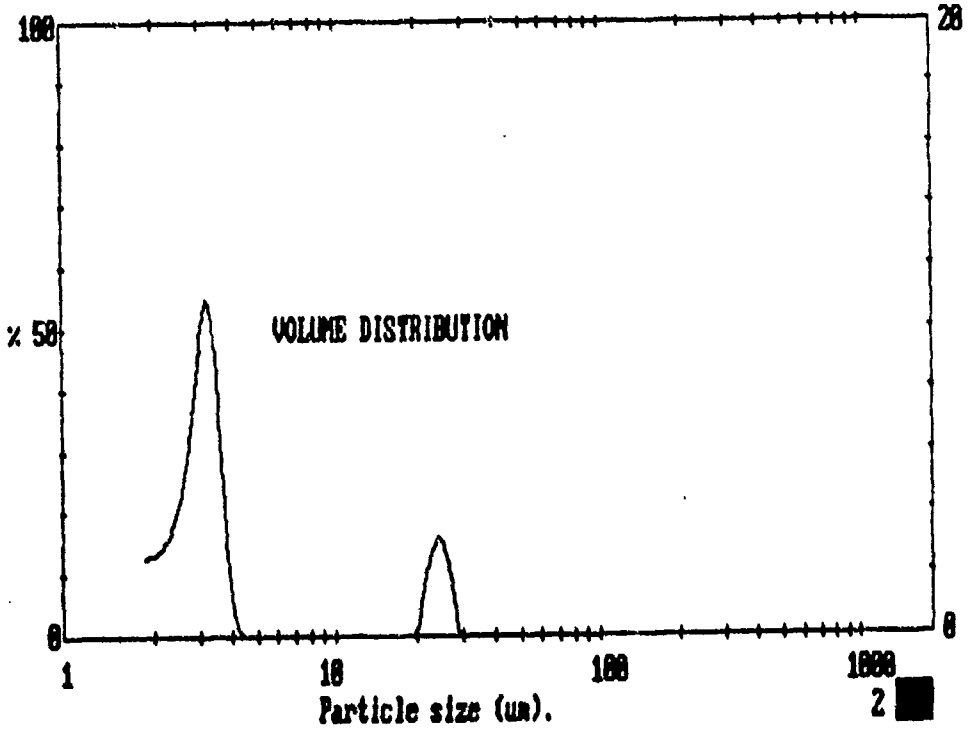


Figure 4.8 Malvern Results of Experiment 2, Run 4

| Upper | in | Lower | Under | Upper | in | Lower | Under | Upper | in | Lower | Under | Span 1.48 |
|---|---|---|---|---|---|---|---|---|---|---|---|---|
| | | | | 57.7 | 0.0 | 49.8 | 100 | 9.82 | 0.0 | 8.47 | 100 | |
| | | | | 49.8 | 0.0 | 43.0 | 100 | 8.47 | 0.0 | 7.30 | 100 | D[4,3] 1.37µm |
| | | | | 43.0 | 0.0 | 37.0 | 100 | 7.30 | 0.0 | 6.30 | 100 | |
| | | | | 37.0 | 0.0 | 32.0 | 100 | 6.30 | 0.0 | 5.43 | 99.9 | |
| 188 | 0.0 | 162 | 100 | 32.0 | 0.0 | 27.5 | 100 | 5.43 | 0.5 | 4.68 | 99.4 | D[3,2] 1.13µm |
| 162 | 0.0 | 140 | 100 | 27.5 | 0.0 | 23.8 | 100 | 4.68 | 1.7 | 4.05 | 97.8 | |
| 140 | 0.0 | 121 | 100 | 23.8 | 0.0 | 20.5 | 100 | 4.05 | 2.8 | 3.48 | 95.0 | |
| 121 | 0.0 | 104 | 100 | 20.5 | 0.0 | 17.7 | 100 | 3.48 | 2.7 | 3.02 | 92.3 | D[v,0.9] 2.59µm |
| 104 | 0.0 | 89.8 | 100 | 17.7 | 0.0 | 15.3 | 100 | 3.02 | 2.2 | 2.60 | 90.1 | |
| 89.8 | 0.0 | 77.5 | 100 | 15.3 | 0.0 | 13.2 | 100 | 2.60 | 4.0 | 2.23 | 86.1 | |
| 77.5 | 0.0 | 66.8 | 100 | 13.2 | 0.0 | 11.4 | 100 | 2.23 | 6.7 | 1.93 | 79.4 | D[v,0.1] 0.72µm |
| 66.8 | 0.0 | 57.7 | 100 | 11.4 | 0.0 | 9.82 | 100 | 1.93 | 79.4 | 0.50 | 0.0 | |
| Source = Data:Input | | | | Beam length = 50.0 mm | | | | Model indp [ 4, 0 ] | | | | D[v,0.5] 1.27µm |
| Focal length = 100 mm | | | | Log. Diff. = 3.668 | | | | | | | | |
| Presentation = pia | | | | Obscuration = 0.5795 | | | | Volume Conc. = 0.0007% | | | | Shape OFF |
| | | | | Volume distribution | | | | Sp.S.A 5.3083 m²/cc. | | | | |

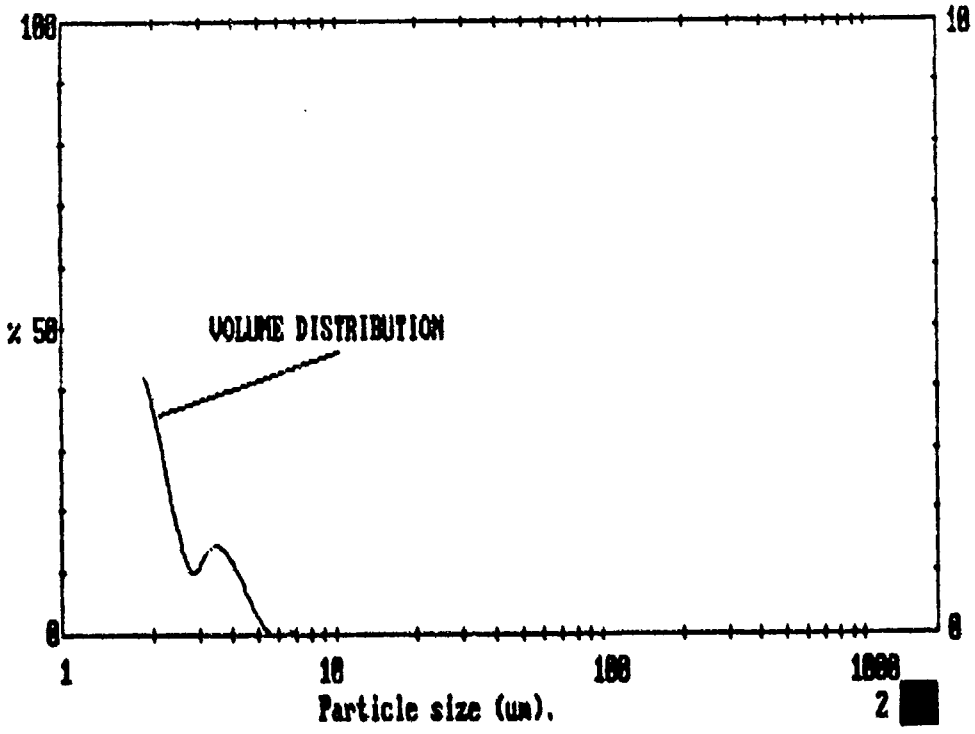


Figure 4.9 Malvern Results of Experiment 2, Run 5

| Upper | in | Lower | Under | Upper | in | Lower | Under | Upper | in | Lower | Under | Span 16.56 |
|---|---|---|---|---|---|---|---|---|---|---|---|---|
| | | | | 57.7 | 0.0 | 49.8 | 100 | 9.82 | 7.7 | 8.47 | 80.2 | |
| | | | | 49.8 | 0.0 | 43.0 | 100 | 8.47 | 5.8 | 7.30 | 74.4 | D[4,3] 4.70µm |
| | | | | 43.0 | 0.0 | 37.0 | 100 | 7.30 | 1.6 | 6.30 | 72.8 | |
| | | | | 37.0 | 0.0 | 32.0 | 100 | 6.30 | 0.5 | 5.43 | 72.3 | |
| 188 | 0.0 | 162 | 100 | 32.0 | 0.2 | 27.5 | 99.8 | 5.43 | 0.3 | 4.68 | 72.0 | D[3,2] 1.32µm |
| 162 | 0.0 | 140 | 100 | 27.5 | 5.5 | 23.8 | 94.3 | 4.68 | 0.0 | 4.05 | 72.0 | |
| 140 | 0.0 | 121 | 100 | 23.8 | 4.6 | 20.5 | 89.7 | 4.05 | 0.0 | 3.48 | 72.0 | |
| 121 | 0.0 | 104 | 100 | 20.5 | 0.0 | 17.7 | 89.7 | 3.48 | 0.0 | 3.02 | 72.0 | D[v,0.9] 20.87µm |
| 104 | 0.0 | 89.8 | 100 | 17.7 | 0.0 | 15.3 | 89.7 | 3.02 | 0.0 | 2.60 | 72.0 | |
| 89.8 | 0.0 | 77.5 | 100 | 15.3 | 0.0 | 13.2 | 89.7 | 2.60 | 0.0 | 2.23 | 72.0 | |
| 77.5 | 0.0 | 66.8 | 100 | 13.2 | 0.0 | 11.4 | 89.7 | 2.23 | 0.3 | 1.93 | 71.7 | D[v,0.1] 0.69µm |
| 66.8 | 0.0 | 57.7 | 100 | 11.4 | 1.9 | 9.82 | 87.8 | 1.93 | 71.7 | 0.50 | 0.0 | |
| Source = Data:Input | | | | Beam length = 50.0 mm | | | | Model indp [ 4, 0 ] | | | | D[v,0.5] 1.22µm |
| | | | | Log. Diff. = 4.266 | | | | | | | | |
| Focal length = 100 mm | | | | Obscuration = 0.3274 | | | | Volume Conc. = 0.0003% | | | | |
| Presentation = pia | | | | Volume distribution | | | | Sp.S.A 4.5387 m²/cc. | | | | Shape OFF |

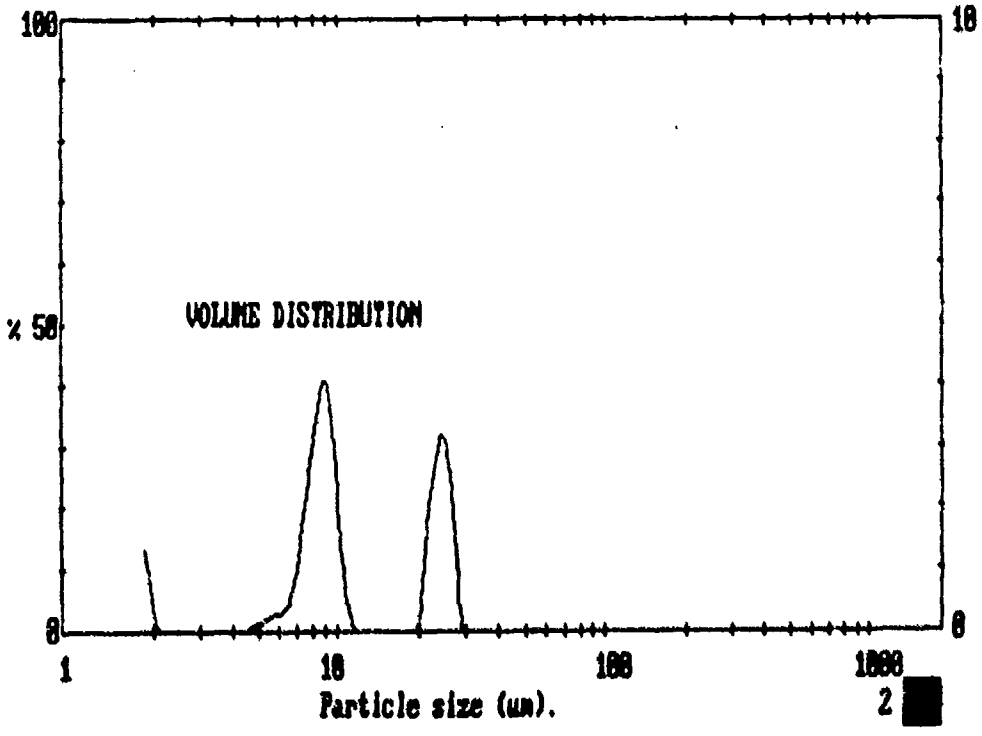


Figure 4.10 Malvern Results of Experiment 3, Run 1

| Upper | in | Lower | Under | Upper | in | Lower | Under | Upper | in | Lower | Under | Span 16.66 |
|---|---|---|---|---|---|---|---|---|---|---|---|---|
| | | | | 57.7 | 0.0 | 49.8 | 100 | 9.82 | 7.2 | 8.47 | 80.1 | |
| | | | | 49.8 | 0.0 | 43.0 | 100 | 8.47 | 4.9 | 7.30 | 75.2 | D[4,3] 4.70µm |
| | | | | 43.0 | 0.0 | 37.0 | 100 | 7.30 | 0.7 | 6.30 | 74.5 | |
| | | | | 37.0 | 0.0 | 32.0 | 100 | 6.30 | 0.2 | 5.43 | 74.2 | |
| 188 | 0.0 | 162 | 100 | 32.0 | 0.2 | 27.5 | 99.8 | 5.43 | 0.3 | 4.68 | 73.9 | D[3,2] 1.31µm |
| 162 | 0.0 | 140 | 100 | 27.5 | 5.3 | 23.8 | 94.5 | 4.68 | 0.0 | 4.05 | 73.9 | |
| 140 | 0.0 | 121 | 100 | 23.8 | 5.4 | 20.5 | 89.0 | 4.05 | 0.0 | 3.48 | 73.9 | |
| 121 | 0.0 | 104 | 100 | 20.5 | 0.3 | 17.7 | 88.8 | 3.48 | 0.0 | 3.02 | 73.9 | D[v,0.9] 21.33µm |
| 104 | 0.0 | 89.8 | 100 | 17.7 | 0.0 | 15.3 | 88.8 | 3.02 | 0.0 | 2.60 | 73.9 | |
| 89.8 | 0.0 | 77.5 | 100 | 15.3 | 0.0 | 13.2 | 88.8 | 2.60 | 0.1 | 2.23 | 73.8 | |
| 77.5 | 0.0 | 66.8 | 100 | 13.2 | 0.0 | 11.4 | 88.8 | 2.23 | 1.4 | 1.93 | 72.4 | D[v,0.1] 0.70µm |
| 66.8 | 0.0 | 57.7 | 100 | 11.4 | 1.5 | 9.82 | 87.3 | 1.93 | 72.4 | 0.50 | 0.0 | |
| Source = Data:Input | | | | Beam length = 50.0 mm | | | | Model indp [ 4, 0 ] | | | | D[v,0.5] 1.24µm |
| Focal length = 100 mm | | | | Log. Diff. = 3.651 | | | | Volume Conc. = 0.0004% | | | | |
| Presentation = pia | | | | Obscuration = 0.3347 | | | | Sp.S.A 4.5951 m²/cc. | | | | Shape OFF |
| | | | | Volume distribution | | | | | | | | |

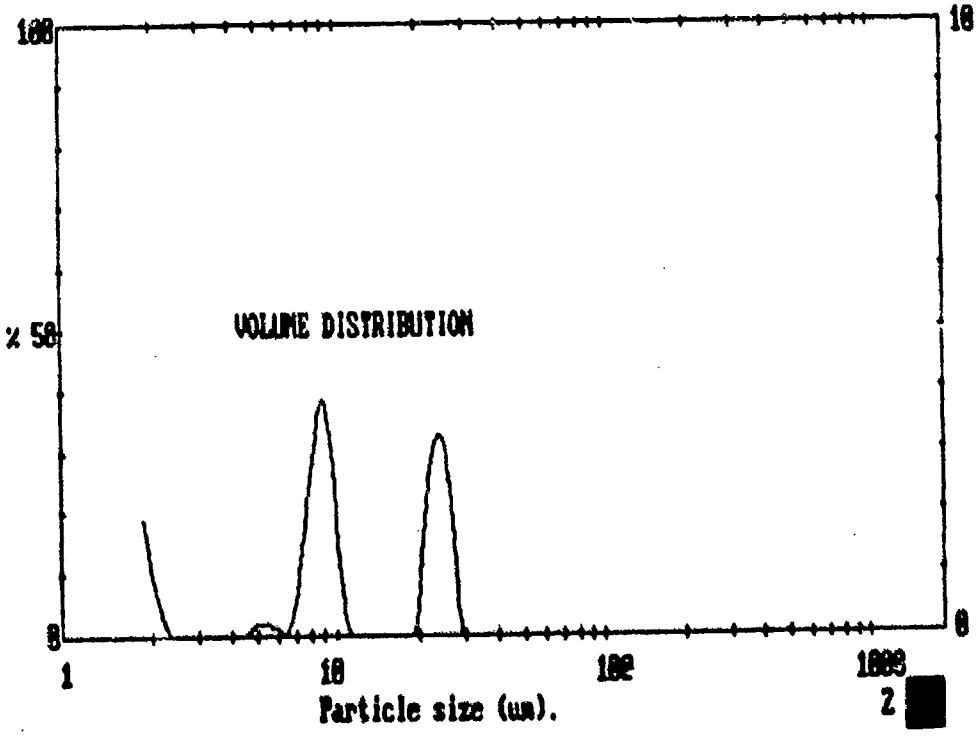


Figure 4.11 Malvern Results of Experiment 3, Run 2

| Upper | in | Lower | Under | Upper | in | Lower | Under | Upper | in | Lower | Under | Span 2.84 |
|---|---|---|---|---|---|---|---|---|---|---|---|---|
| | | | | 57.7 | 0.0 | 49.8 | 100 | 9.82 | 1.2 | 8.47 | 92.6 | |
| | | | | 49.8 | 0.0 | 43.0 | 100 | 8.47 | 1.2 | 7.30 | 91.4 | D[4,3] 2.94µm |
| | | | | 43.0 | 0.0 | 37.0 | 100 | 7.30 | 0.8 | 6.30 | 90.6 | |
| | | | | 37.0 | 0.0 | 32.0 | 100 | 6.30 | 0.5 | 5.43 | 90.1 | |
| 188 | 0.0 | 162 | 100 | 32.0 | 0.1 | 27.5 | 99.9 | 5.43 | 0.3 | 4.68 | 89.8 | D[3,2] 1.32µm |
| 162 | 0.0 | 140 | 100 | 27.5 | 2.7 | 23.8 | 97.1 | 4.68 | 0.3 | 4.05 | 89.5 | |
| 140 | 0.0 | 121 | 100 | 23.8 | 2.1 | 20.5 | 95.0 | 4.05 | 0.3 | 3.48 | 89.1 | |
| 121 | 0.0 | 104 | 100 | 20.5 | 0.0 | 17.7 | 95.0 | 3.48 | 2.6 | 3.02 | 86.5 | D[v,0.9] 5.09µm |
| 104 | 0.0 | 89.8 | 100 | 17.7 | 0.0 | 15.3 | 95.0 | 3.02 | 7.7 | 2.60 | 78.9 | |
| 89.8 | 0.0 | 77.5 | 100 | 15.3 | 0.0 | 13.2 | 95.0 | 2.60 | 8.6 | 2.23 | 70.3 | |
| 77.5 | 0.0 | 66.8 | 100 | 13.2 | 0.4 | 11.4 | 94.6 | 2.23 | 7.0 | 1.93 | 63.3 | D[v,0.1] 0.76µm |
| 66.8 | 0.0 | 57.7 | 100 | 11.4 | 0.8 | 9.82 | 93.8 | 1.93 | 63.3 | 0.50 | 0.0 | |
| Source = Data:Input | | | | Beam length = 50.0 mm | | | | Model indp [ 4, 0 ] | | | | D[v,0.5] 1.52µm |
| | | | | Log. Diff. = 2.730 | | | | | | | | |
| Focal length = 100 mm | | | | Obscuration = 0.3661 | | | | Volume Conc. = 0.0004% | | | | |
| Presentation = pia | | | | Volume distribution | | | | Sp.S.A 4.5522 m²/cc. | | | | Shape OFF |

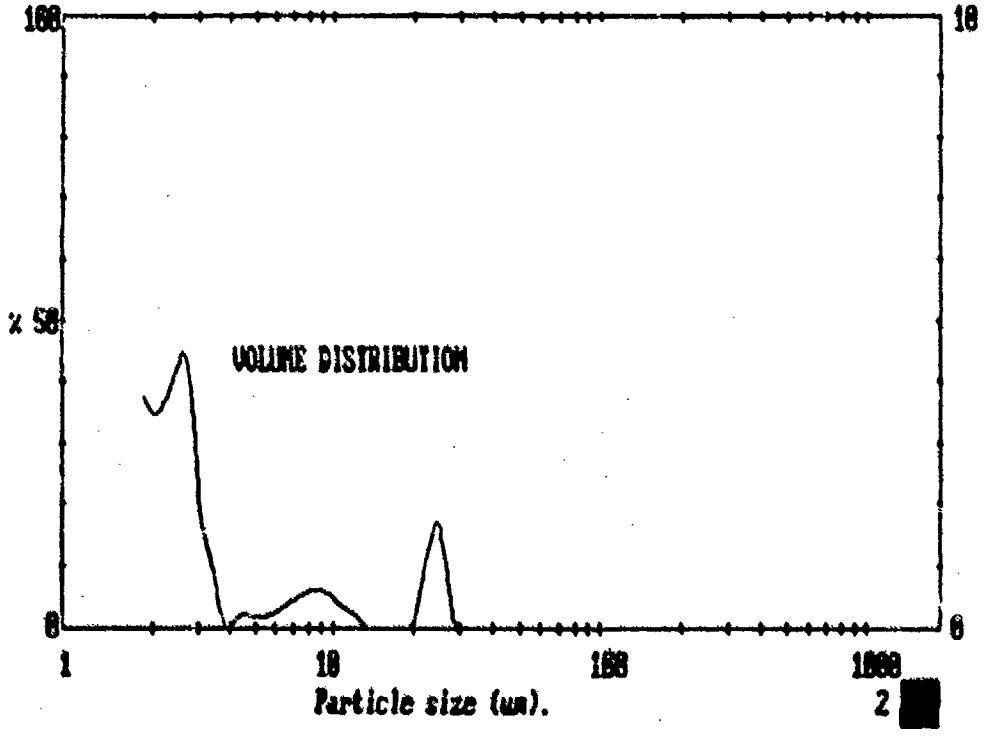


Figure 4.12 Malvern Results of Experiment 4, Run 1

| Upper | in | Lower | Under | Upper | in | Lower | Under | Upper | in | Lower | Under | Span 7.20 |
|---|---|---|---|---|---|---|---|---|---|---|---|---|
| | | | | 57.7 | 0.0 | 49.8 | 100 | 9.82 | 0.0 | 8.47 | 85.8 | |
| | | | | 49.8 | 0.0 | 43.0 | 100 | 8.47 | 0.0 | 7.30 | 85.3 | D[4,3] 4.62µm |
| | | | | 43.0 | 0.0 | 37.0 | 100 | 7.30 | 0.0 | 6.30 | 85.8 | |
| | | | | 37.0 | 0.0 | 32.0 | 100 | 6.30 | 0.0 | 5.43 | 85.8 | |
| 188 | 0.0 | 162 | 100 | 32.0 | 0.0 | 27.5 | 100 | 5.43 | 0.6 | 4.68 | 85.2 | D[3,2] 1.77µm |
| 162 | 0.0 | 140 | 100 | 27.5 | 0.7 | 23.8 | 99.3 | 4.68 | 3.1 | 4.05 | 82.1 | |
| 140 | 0.0 | 121 | 100 | 23.8 | 4.4 | 20.5 | 94.9 | 4.05 | 6.2 | 3.48 | 75.9 | |
| 121 | 0.0 | 104 | 100 | 20.5 | 7.1 | 17.7 | 87.7 | 3.48 | 9.3 | 3.02 | 66.5 | D[v,0.9] 18.64µm |
| 104 | 0.0 | 89.8 | 100 | 17.7 | 1.9 | 15.3 | 85.8 | 3.02 | 12.6 | 2.60 | 54.0 | |
| 89.8 | 0.0 | 77.5 | 100 | 15.3 | 0.0 | 13.2 | 85.8 | 2.60 | 9.9 | 2.23 | 44.1 | |
| 77.5 | 0.0 | 66.8 | 100 | 13.2 | 0.0 | 11.4 | 85.8 | 2.23 | 5.5 | 1.93 | 38.6 | D[v,0.1] 0.88µm |
| 66.8 | 0.0 | 57.7 | 100 | 11.4 | 0.0 | 9.82 | 85.8 | 1.93 | 38.6 | 0.50 | 0.0 | |
| Source = Data:Input | | | | Beam length = 50.0 mm | | | | Model indp [ 4, 0 ] | | | | D[v,0.5] 2.47µm |
| Focal length = 100 mm | | | | Log. Diff. = 3.575 | | | | | | | | |
| Presentation = pia | | | | Obscuration = 0.4081 | | | | Volume Conc. = 0.0006% | | | | |
| | | | | Volume distribution | | | | Sp.S.A 3.3944 m²/cc. | | | | Shape OFF |

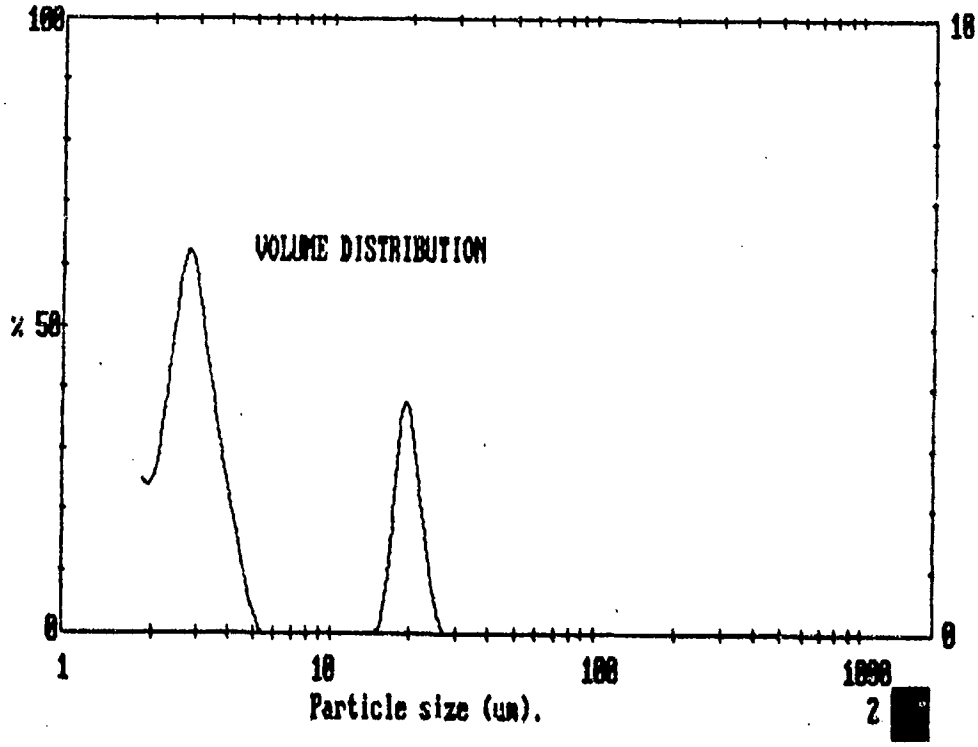


Figure 4.13 Malvern Results of Experiment 4, Run 2

| Upper | in | Lower | Under | Upper | in | Lower | Under | Upper | in | Lower | Under | Span |
|---|---|---|---|---|---|---|---|---|---|---|---|---|
| | | | | 57.7 | 0.0 | 49.8 | 100 | 9.82 | 0.0 | 8.47 | 81.9 | 12.82 |
| | | | | 49.8 | 0.0 | 43.0 | 100 | 8.47 | 0.0 | 7.30 | 81.9 | D[4,3] |
| | | | | 43.0 | 0.0 | 37.0 | 100 | 7.30 | 0.0 | 6.30 | 81.9 | 5.76µm |
| | | | | 37.0 | 0.0 | 32.0 | 100 | 6.30 | 0.0 | 5.43 | 81.8 | |
| 188 | 0.0 | 162 | 100 | 32.0 | 0.4 | 27.5 | 99.6 | 5.43 | 0.3 | 4.68 | 81.5 | D[3,2] |
| 162 | 0.0 | 140 | 100 | 27.5 | 10.0 | 23.8 | 89.5 | 4.68 | 1.4 | 4.05 | 80.1 | 1.53µm |
| 140 | 0.0 | 121 | 100 | 23.8 | 7.7 | 20.5 | 81.9 | 4.05 | 4.6 | 3.48 | 75.4 | |
| 121 | 0.0 | 104 | 100 | 20.5 | 0.0 | 17.7 | 81.9 | 3.48 | 6.1 | 3.02 | 69.3 | D[v,0.9] |
| 104 | 0.0 | 89.8 | 100 | 17.7 | 0.0 | 15.3 | 81.9 | 3.02 | 5.1 | 2.60 | 64.3 | 23.96µm |
| 89.8 | 0.0 | 77.5 | 100 | 15.3 | 0.0 | 13.2 | 81.9 | 2.60 | 5.1 | 2.23 | 59.1 | |
| 77.5 | 0.0 | 66.8 | 100 | 13.2 | 0.0 | 11.4 | 81.9 | 2.23 | 5.9 | 1.93 | 53.2 | D[v,0.1] |
| 66.8 | 0.0 | 57.7 | 100 | 11.4 | 0.0 | 9.82 | 81.9 | 1.93 | 53.2 | 0.50 | 0.0 | 0.80µm |
| Source = Data:Input | | | | Beam length = 50.0 mm | | | | Model indp [ 4, 0 ] | | | | D[v,0.5] |
| | | | | Log. Diff. = 3.679 | | | | | | | | 1.80µm |
| Focal length = 100 mm | | | | Obscuration = 0.4601 | | | | Volume Conc. = 0.0006% | | | | |
| Presentation = pia | | | | Volume distribution | | | | Sp.S.A 3.9093 m²/cc. | | | | Shape OFF |

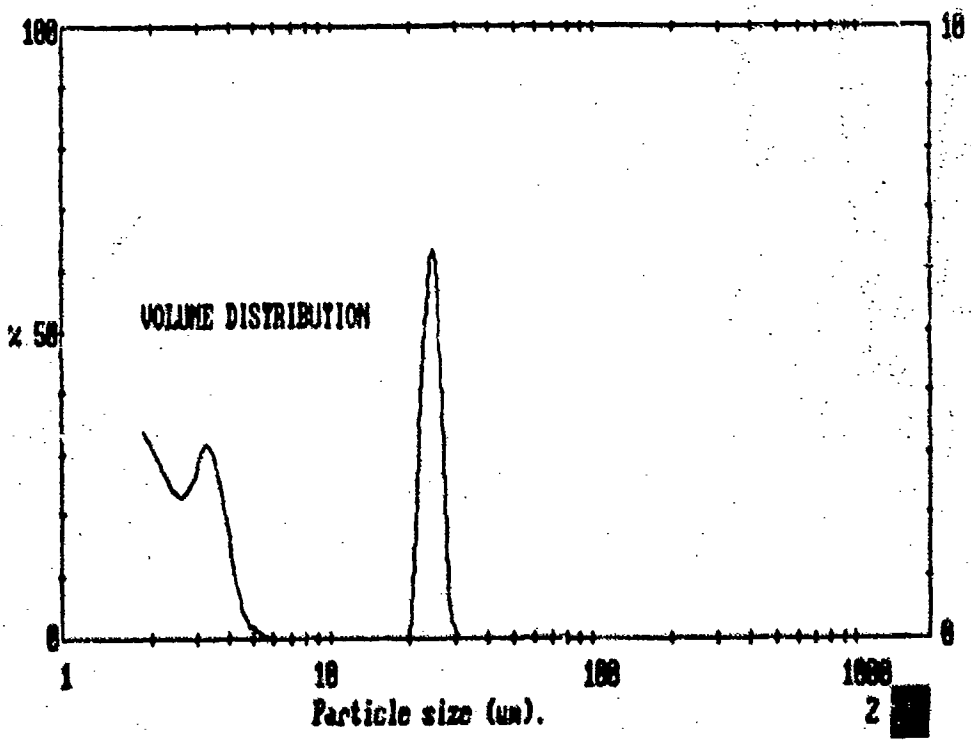


Figure 4.14 Malvern Results of Experiment 4, Run 3

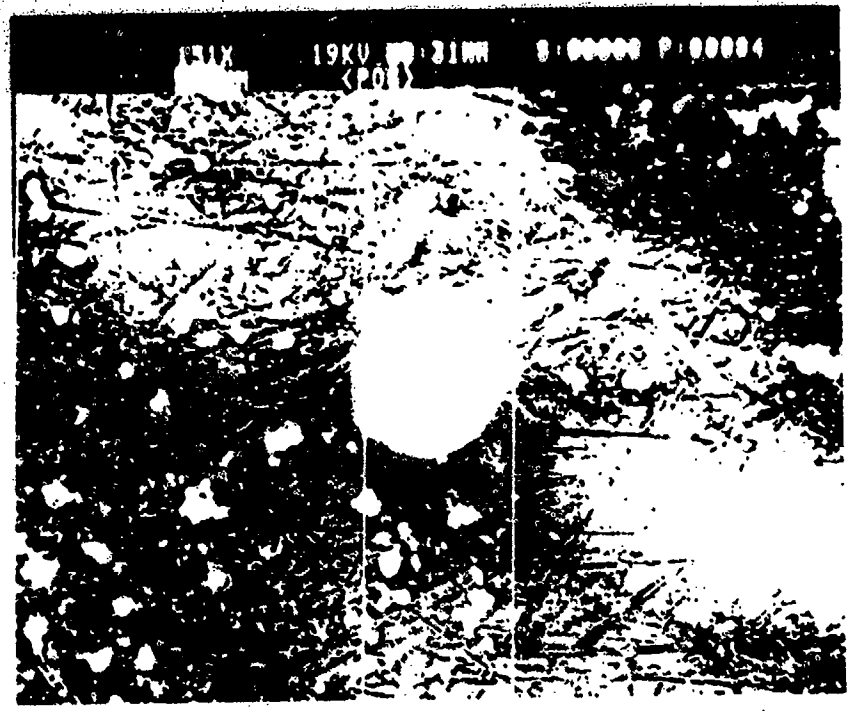

Figure 4.15 Example SEM Picture of a 137 μ Diameter $Al_2O_3$ Particle Above the Submerged Nozzle

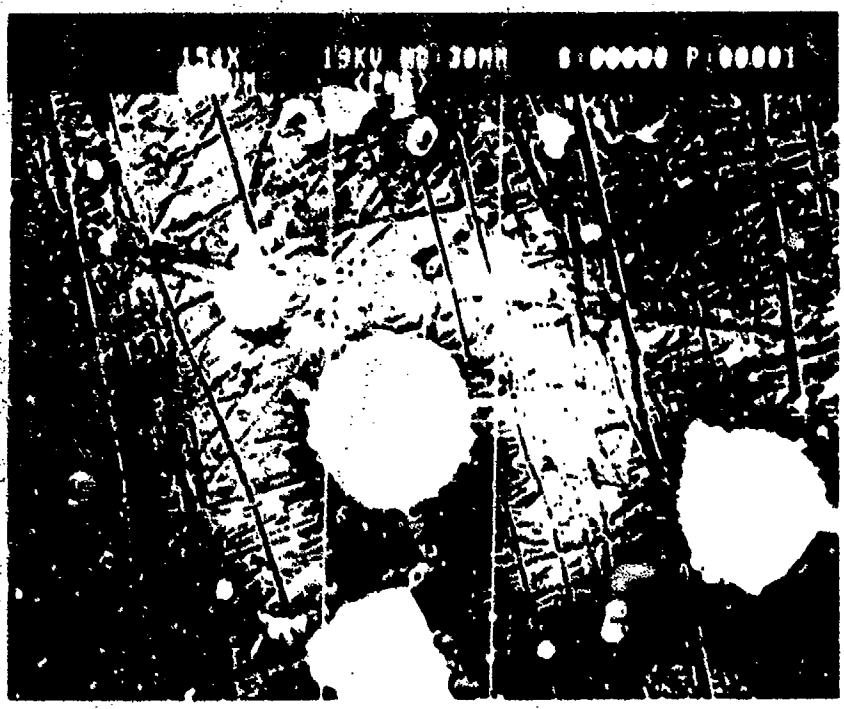

Figure 4.16 Example SEM Picture of a 148 μ Diameter $Al_2O_3$ Particle Above the Submerged Nozzle

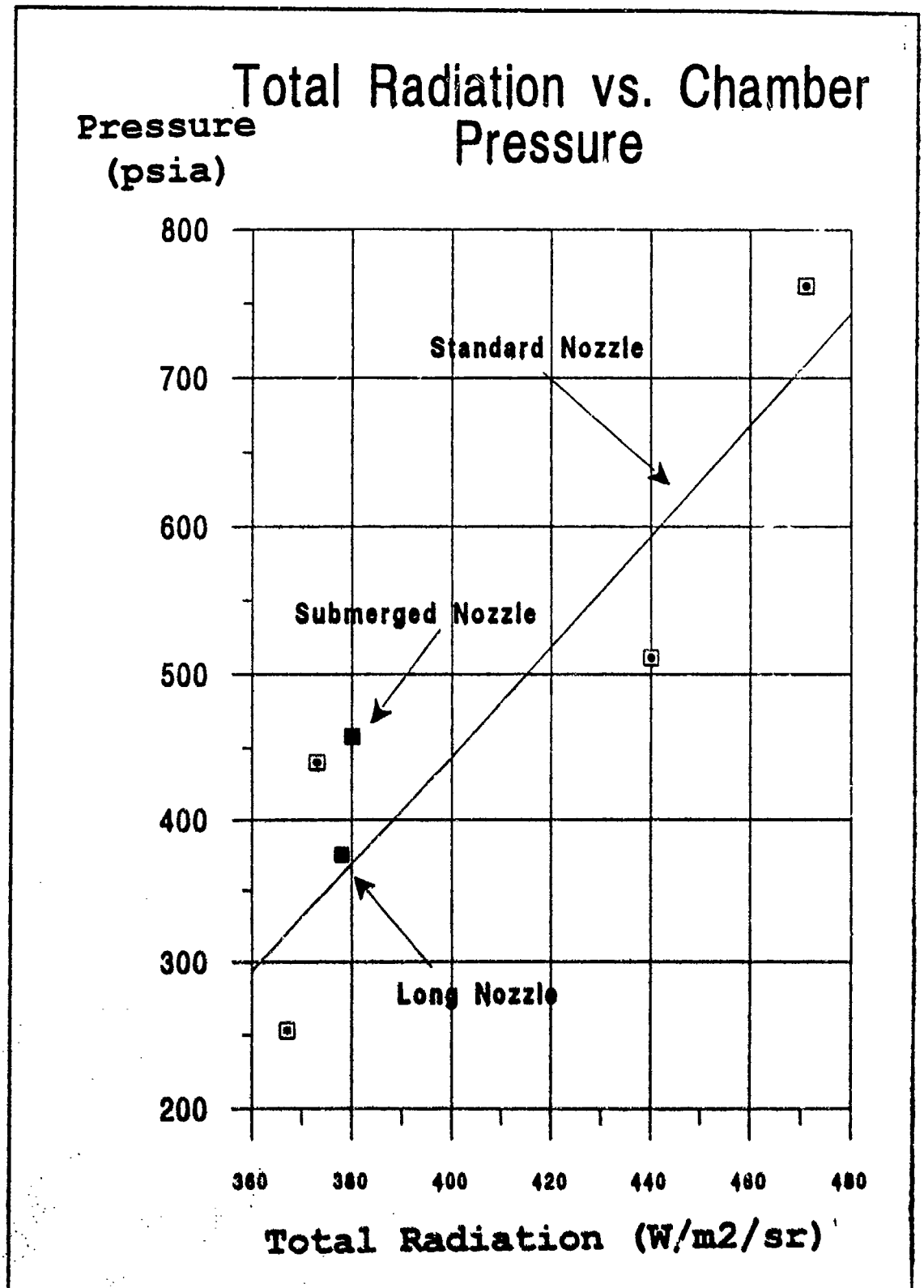


Figure 4.17 Total Radiation of Different Plume Samples vs Chamber Pressure Sketch

## LIST OF REFERENCES


1. Propulsion, Smith, P.K., Advisory Group For Aerospace Research and Development (AGARD) Lecture Series 188, AGARD-LS-188, "Rocket Motor Plume Technology", June 1993.

2. Reed, R.A. and Calia, V.S., "Review of Aluminum Oxide Rocket Exhaust Particles", AIAA 28th Thermophysics Conference, July 6-9, 1993, Orlando,FL.

3. Braithwaite, P.C., Christensen, W.N. and Daugherty, V., "Quench Bomb Investigation of Aluminum Oxide Formation from Solid Rocket Propellants, Part 1:Experimental Methodology", 25th JANNAF Combustion Meeting Vol. 1 NASA-MARSHALL Space Flight Center Huntsville, Alabama 24-28 October 1988, pp.175-184.

4. Salita, M., "Characterization of $Al_2O_3$ Particulate Formed During Combustion of SRB Propellant (TP-H1148)", Morton Thiokol Inc. Space Division, Report No. TWR-18456, 13 September 1988.

5. "Solid Propellant Selection and Characterization", NASA SP-8064, June 1971.

6. Laredo, D., McCroie II, J.D., Vaughn, J.K. and Netzer, D.W., "Motor and Plume Particle Size Measurements in Solid Propellant Micromotors", Accepted for Publication in J. Propulsion and Power, 1993.

7. Pilch, M., Erdman, C. A., "Use of Breakup Time Data and Velocity History Data to Predict the Maximum Size of Stable Fragments For Acceleration-Induced Breakup of a Liquid Drop", Int. J. Multiphase Flow, Vol. 13, No.6, 1987, pp 741-757.

8. Malvern Instruments Ltd., "Malvern 2600 Instruction Manual",Spring Lane South, Malvern, England.

9. Traineau, J.C., Kuentzmann, P., Prevost, M., Tarrin, P. and Delfour, A., "Particle Size Distribution Measurements in a Subscale Motor for the Ariane 5 Solid Rocket Booster", AIAA 92-3049, 28th Joint Propulsion Conference and Exhibit, 6-8 July 1992, Nashville, TN.

10. AEROMETRICS "Laser Doppler Velocimeter Doppler Signal Analyzer One-Component User's Manual", April 1993.

11. Gomes, P.V., "The Validation and Implementation of Optical Diagnostics for Particle Sizing in Rocket Motors", Master's Thesis, Naval Postgraduate School, Monterey, California, December 1993.

12. AGEMA Infrared Systems, "Thermovision 800 Introductory Manual", Rev. 3, June 1992.

13. NASA Space Vehicle Design Criteria, "Solid Rocket Motor Nozzles", NASA SP-8115, June 1975.

14. Gülder, Ö.L., "Multiple Scatttering Effects in Drop Sizing of Dense Fuel Sprays by Laser Diffraction", PEP Paper # 70-7, NATO/AGARD 70th Symposium of the Propulsion and Energetics Panel on Combustion and Fuels in Gas Turbine Engines, 19-23 October 1987, Chania (Crete), Greece.

15. Cambridge Instruments Limited "Stereoscan 200 Scanning Electron Microscope Operating Instructions", 3 April 1985.

## INITIAL DISTRIBUTION LIST

| | | No. Copies |
|---|---|---|
| 1. | Defense Technical Information Center<br>Cameron Station<br>Alexandria VA 22304-6145 | 2 |
| 2. | Library, Code 052<br>Naval Postgraduate School<br>Monterey CA 93943-5002 | 2 |
| 3. | Department Chairman, Code AA<br>Department of Aeronautics and Astronautics<br>Naval Postgraduate School<br>Monterey, California 93943-5004 | 1 |
| 4. | Professor D.W. Netzer, Code AA/Nt<br>Department of Aeronautics and Astronautics<br>Naval postgraduate School<br>Monterey, California 93943-5004 | 2 |
| 5. | Professor J.V. Sanders, Code PH/Sd<br>Department of Physics<br>Naval Postgraduate School<br>Monterey, California 93943-5004 | 1 |
| 6. | Gölcük Tersanesi Komutanligi<br>Gölcük, Kocaeli, Turkey | 2 |
| 7. | Taskizak Tersanesi Komutanligi<br>Haskôy, Istanbul, Turkey | 2 |
| 8. | Deniz Harp Okulu Komutanligi<br>Tuzla, Istanbul, Turkey | 1 |
| 9. | Dz.K.K.ligi Personel Egt. D. Bsk.ligi<br>Bakanliklar, Ankara, Turkey | 1 |
| 10. | Bülent Yakin<br>Salacak Iskele Cad. No:42/4<br>81160 Üsküdar, Istanbul, Turkey | 1 |